Tectonophysics 775 (2020) 228310

Contents lists available at ScienceDirect

Tectonophysics

journal homepage: www.elsevier.com/locate/tecto

Diachronous uplift in intra-continental orogeny: 2D thermo-mechanical modeling of the India-Asia collision

Shuang Bian[a,b], Junfeng Gong[a,b,*], Lin Chen[c,*], Andrew V. Zuza[d], Hanlin Chen[a,b], Xiubin Lin[a,b], Xiaogan Cheng[a,b], Rong Yang[a,b]

[a] School of Earth Sciences, Zhejiang University, Hangzhou 310027, China
[b] Research Center for Structures in Oil and Gas Bearing Basins, Ministry of Education, Hangzhou 310027, China
[c] Institute of Geology and Geophysics, Chinese Academy of Sciences, Beijing 100029, China
[d] Nevada Bureau of Mines and Geology, University of Nevada, Reno, NV 89557, USA

ARTICLE INFO

Keywords:
Diachronous uplift
Thermo-mechanical modeling
India-Asia collision
Far-field stress transfer
West Kunlun
Tian Shan

ABSTRACT

The Cenozoic India-Asia collision reactivated several ancient thrust belts in the interior of the Asian continent, including the West and East Kunlun ranges in central Tibet, and the Tian Shan and Qilian Shan further north. Both basin sedimentary records and thermochronological data show that the uplift of the South Tian Shan and Qilian Shan at the north occurred earlier than that of the West and East Kunlun ranges at the south. Diachronous continental deformation and initiation of uplift during orogeny are contrary to the general notion that the stress transfer in response to the India-Asia collision should propagate sequentially from south to north. Here we systematically conducted 2D thermo-mechanical simulations to investigate possible factors for this diachronous deformation pattern. The results show that a hotter Tian Shan lithosphere, with Moho temperature > 100 °C hotter than that of the proto-southern Asia, leads to an earlier and higher uplift of the Tian Shan. Additionally, a faster convergence rate of the India-Asia collision results in a more efficient transfer of boundary force into the upper plate's interior, giving rise to a larger amount of uplift in the Tian Shan. We conclude that intra-continental ranges with weaker lithosphere, such as the Tian Shan or Qilian Shan, uplift earlier than stronger regions, such as the West and East Kunlun ranges. Faster convergence rates amplify this situation. Our results imply that the unique diachronous growth of the Tibetan plateau arises from its complex pre-collisional history, which includes collided arc-continent terranes with hotter and weaker lithosphere that respond to the effects of far-field stress transfer.

1. Introduction

The Cenozoic India-Asia collision exerts far-field effects on the tectonic deformation of the interior of Asian plate, and boundary forces along the collisional margin have reactivated several weakly welded suture zones in southern Asia (Hendrix et al., 1992; Yin, 2000; Yin and Harrison, 2000; Zuza and Yin, 2017). This proposal has been related to the stepwise growth of the Tibetan plateau from south to north (England and Houseman, 1986; Tapponnier et al., 2001). Stress resulting from the collision was transferred northward through the Tibetan plateau, Tarim basin and Qaidam basin to the interior of Asian plate, leading to deformation and uplift of the Tian Shan and Qilian Shan thrust belts, strike-slip faulting in Mongolia, and the formation of the Baikal rift (Molnar and Tapponnier, 1975; Tapponnier et al., 1982; Vassallo et al., 2007; De Grave et al., 2007).

Past research commonly highlights the expected northward propagation of deformation and northward younging of orogeny in response to the India-Asia collision. However, this idea has been challenged over the years by observations from both basin-sedimentation studies and bedrock thermochronology, which demonstrate that uplift occurred relatively early along the orogen's northernmost boundaries, prior to regions within the plateau interior. Specifically, the South Tian Shan in the north uplifted prior to the West Kunlun range in the south, and uplift of the Qilian Shan in the north preceded that of the East Kunlun range in the south (Fig. 1, Supplementary Data Table A.1). This out-of-sequence uplift of the Himalayan-Tibetan orogen conflicts with the aforementioned long-held notion of progressive northward propagation. It is therefore critical to understand the mechanism for the unique diachronous orogeny of the Tibetan plateau and thrust belts in Asian continent's interior under the framework of India-Asia collision.

* Corresponding authors.
E-mail addresses: jfgong@zju.edu.cn (J. Gong), chenlin@mail.iggcas.ac.cn (L. Chen).

https://doi.org/10.1016/j.tecto.2019.228310
Received 13 June 2019; Received in revised form 9 December 2019; Accepted 14 December 2019
Available online 19 December 2019
0040-1951/

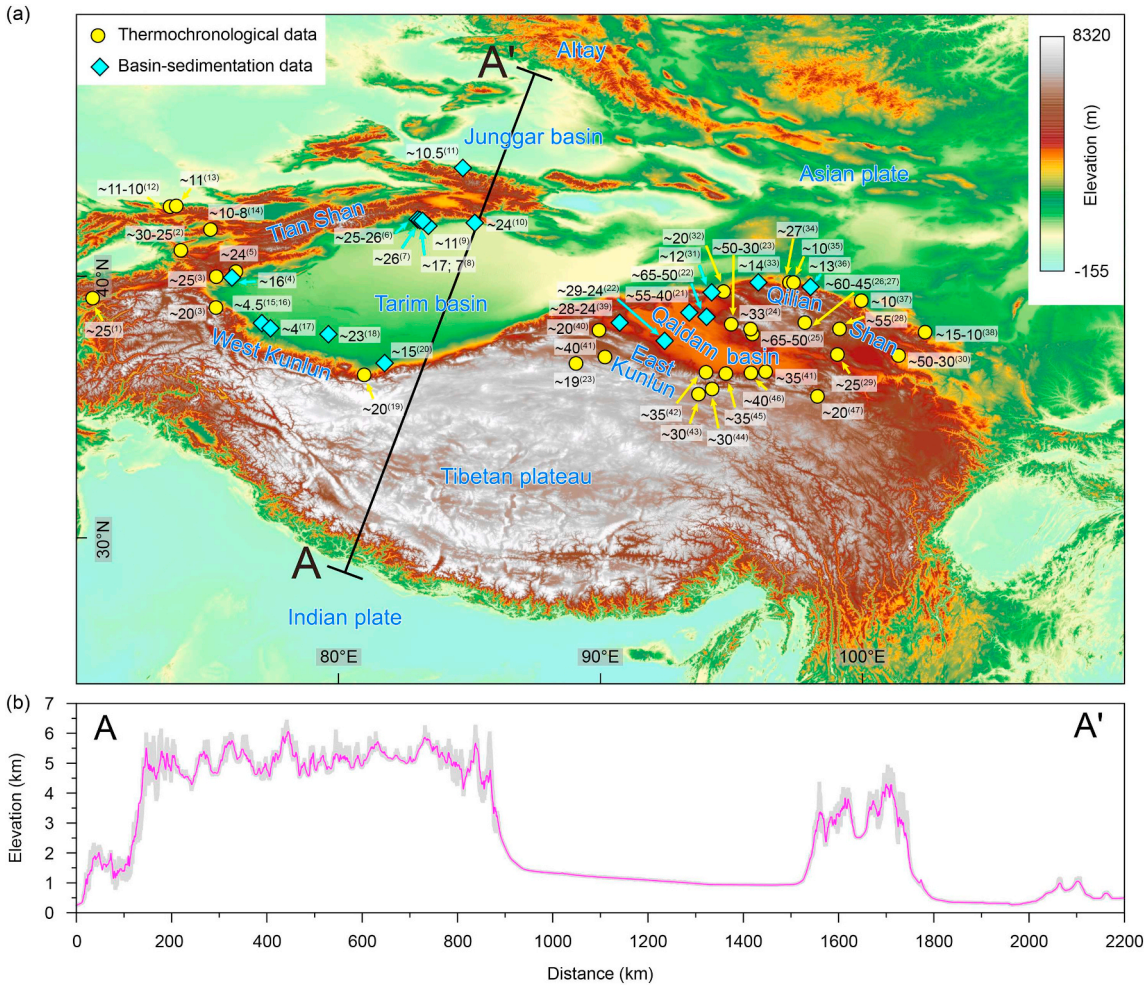

Fig. 1. (a) Topographic map of the Tibetan plateau and surrounding region. A-A′ indicates the location of topographic profile in panel b. Numbers are uplift or deformation timing in million years, and those in brackets are reference numbers. The South Tian Shan uplifted at ~26–24 Ma (references: (1) Jepson et al., 2017; (2) Glorie et al., 2011; (3) Sobel and Dumitru, 1997; (5) Sobel et al., 2006; (6) Wang et al., 2011; (7) Li et al., 2019b; (10) Yin et al., 1998) with multi-phase uplifting pulses at ~17–16 Ma and younger (references: (4) Heermance et al., 2007; (8) Huang et al., 2006; (9) Charreau et al., 2006). The North Tian Shan uplifted at ~11 Ma (references: (11) Charreau et al., 2005; (12) Bullen et al., 2003; (13) Bullen et al., 2001; (14) Glorie et al., 2010). The West Kunlun range uplifted at ~23–15 Ma (references: (3) Sobel and Dumitru, 1997; (18) Jiang and Li, 2014; (19) Wang et al., 2003b; (20) Li et al., 2011) with a later stage of uplift at ~4.5 Ma (references: (15) Zheng et al., 2000; (16) Zheng et al., 2006; (17) Tada et al., 2010). The Qilian Shan uplifted at ~65–30 Ma (references: (21) Zhuang et al., 2011; (22) Yin et al., 2008; (23) Jolivet et al., 2001; (24) Yin et al., 2002; (25) Zhuang et al., 2018; (26) Zuza et al., 2016; (27) Zuza et al., 2019; (28) Qi et al., 2016; (29) Lu et al., 2012; (30) Zhang et al., 2015) with a more recent phase of deformation at ~20–10 Ma (References: (31) Wang et al., 2003a; (32) Shi et al., 2018; (33) Sun et al., 2005; (34) Guo et al., 2009; (35) Zheng et al., 2017; (36) Bovet et al., 2009; (37) Zheng et al., 2010; (38) Li et al., 2019a). The East Kunlun range uplifted at 40–20 Ma (references: (22) Yin et al., 2008; (23) Jolivet et al., 2001; (39) Yin et al., 2007; (40) Wu et al., 2019; (41) Wang et al., 2017; (42) Wang et al., 2004; (43) Duvall et al., 2013; (44) Mock et al., 1999; (45) Clark et al., 2010; (46) Wang et al., 2016; (47) Yuan et al., 2006). (b) Topography of a 20-km-wide swath profile along A-A′, displaying a topographical pattern with high-low-high-low feature.

Intra-continental deformation within the India-Asia collision has been extensively studied by numerical modeling over the past four decades. Previous studies were mainly based on thin viscous sheet models (England and Houseman, 1985, 1986; Neil and Houseman, 1997; Dayem et al., 2009) or viscoplastic models under plane strain conditions (e.g., Vilotte et al., 1984). These models highlighted the importance of a rigid inclusion, analogous to the Tarim basin, to drive crustal thickening in northern Tibet or the Tian Shan. Recently, Pusok and Kaus (2015) used 3D mechanical models to show that both external forcing and the presence of a strong block (i.e., Tarim basin) are necessary to generate high topographic fronts and plateaus. Some models take into account the south-north rheological heterogeneity to investigate the dynamics of the multi-terrane configuration of the Tibetan plateau (Kelly et al., 2016; Li et al., 2016; Huangfu et al., 2018). These models emphasize that distinct properties of the multiple terranes played an important role in the geodynamic evolution of the Tibetan plateau and associated intraplate orogeny. However, none of these previous studies investigated the cause for the out-of-sequence uplift observed in the Asian plate and/or the Himalayan-Tibetan orogen, including any potential influence of terrane variability on its coupled thermal and mechanical evolution.

In this study, we investigate the far-field effects of the India-Asia collision on intraplate orogeny using 2D thermo-mechanical simulations. Our focus is on the topographic expression in response to the collision between the Indian and Asian lithosphere with varying strength heterogeneity. Lithospheric strength variation here is expressed in terms of lithospheric thermal state or rheology contrast (e.g., Chen and Gerya, 2016; Chen et al., 2017). On this basis, two key parameters are systematically examined: (1) convergence rate and (2) the upper plate thermal state. The aim of this study is not to reproduce the orogeny in detail, but rather to advance our understanding of potential driving mechanism for the diachronous topographic rise of the West Kunlun range versus the South Tian Shan, which also provides insights for the out-of-sequence deformation observed between the East

Kunlun range and Qilian Shan.

2. Uplift timing of thrust belts in the interior of Asian plate

In discussing the diachronous uplift across the Tibetan plateau, we focus on two north-south profiles: in the west is the West Kunlun-South Tian Shan and in the east is the East Kunlun-Qilian Shan (Fig. 1a, Supplementary Data Table A.1). In the West Kunlun range (i.e., the northwestern margin of the Tibetan plateau south of Tarim basin), the initiation of uplift is constrained at ~23 Ma based on the development of a foreland basin in the southern Tarim basin, which is identified as an environment transition between marine carbonate platform and clastic tidal flat (Jiang and Li, 2014). This constraint is in accordance with the estimated ~20–15 Ma initiation age based on apatite fission track (AFT) dating (Sobel and Dumitru, 1997; Cowgill, 2001; Wang et al., 2003b), multi-thermochronometer research (Ritts et al., 2008) and Nd isotopic analysis (Li et al., 2011). In addition, a later stage of uplift has been estimated at ~4.5 Ma constrained by paleo-environmental analyses (Zheng et al., 2000, 2006; Tada et al., 2010).

In contrast, the South Tian Shan, further to the north of the West Kunlun range and Tarim basin, is characterized by ~26–24 Ma initial uplift and subsequent multi-phase uplifting pulses. Near the South Tian Shan front, growth strata and the transition of sedimentary facies in the Kuche basin recorded initial deformation at ~26–25 Ma (Wang et al., 2011; Li et al., 2019b) and ~24–21 Ma (Yin et al., 1998), respectively. These constraints are confirmed by thermochronology research (i.e., AFT, and apatite and zircon (U-Th)/He), which suggests uplift and related exhumation initiated at ~25 Ma (Hendrix et al., 1994; Sobel and Dumitru, 1997; Sobel et al., 2006, 2013; Glorie et al., 2011; Jepson et al., 2017). Subsequently, the South Tian Shan underwent the main phase of uplift at ~16–15 Ma based on estimates of total crustal shortening using modern deformation rates (Avouac et al., 1993), the acceleration of sediment flux (Métivier and Gaudemer, 1997), and an increase in sedimentation rate (Huang et al., 2006; Heermance et al., 2007). A later pulse of intensified uplift is also recognized in the Late Miocene-Pliocene (Charreau et al., 2006, 2009; Huang et al., 2006; Tang et al., 2011; Zhang et al., 2014). In addition, the surface uplift of the North Tian Shan and Kyrgyz North Tian Shan initiated at ~11 Ma possibly due to the migration of compressional stress (Bullen et al., 2001, 2003; Charreau et al., 2005; Glorie et al., 2010). In summary, the initial uplift of the South Tian Shan is earlier than that of the West Kunlun range by ~2–3 Myr, although both the South and North Tian Shan experienced distinct late Cenozoic deformation histories.

On the East Kunlun-Qilian Shan profile, to the east of the West Kunlun-Tian Shan profile, deformation and uplift also exhibited multiple episodes. In the East Kunlun range, local Cenozoic exhumation initiated at ~40–35 Ma (Wang et al., 2004, 2016, 2017; Clark et al., 2010). This was followed by a subsequent primary phase of uplift beginning at ~29–24 Ma as documented by the growth strata in the southern Qaidam basin (Yin et al., 2007, 2008; Wu et al., 2014; Cheng et al., 2016, 2018). This history has been supported by numerous thermochronology studies. For instance, $^{40}Ar/^{39}Ar$ and apatite (U-Th)/He ages recorded a deformation at ~30–20 Ma (Mock et al., 1999; Liu et al., 2005; Duvall et al., 2013); AFT dating documented a later stage of rapid cooling event at ~20–10 Ma (Lewis, 1990; Yuan et al., 2003, 2006; McRivette et al., 2019; Wu et al., 2019).

In the Qilian Shan, combined thermochronology, sedimentology and structural studies suggest that Cenozoic uplift and exhumation initiated at ~65–50 Ma (Jolivet et al., 2001; Yin et al., 2008; Zhuang et al., 2011, 2018; Zhang et al., 2015; Qi et al., 2016; Zuza et al., 2016, 2019; Li et al., 2019c). Subsequently, a more recent phase of deformation and exhumation occurred in the Miocene time at ~20–10 Ma (Wang et al., 2003a; Sun et al., 2005; Bovet et al., 2009; Guo et al., 2009; Zheng et al., 2010, 2017; Shi et al., 2018; Li et al., 2019a), probably related to the initiation of strike-slip faulting in northern Tibet (Duvall et al., 2013; Zuza and Yin, 2016; Li et al., 2019a). In summary, the Qilian Shan uplifted at least 10 Myr earlier than the East Kunlun range, and possibly > 20 Myr earlier, which clearly demonstrates a diachronous uplift pattern on the East Kunlun-Qilian Shan profile.

3. Numerical modeling method

3.1. Governing equations

To explore the far-field effect of the India-Asia collision, we use the 2D thermo-mechanical code, I2VIS (Gerya and Yuen, 2003a). It solves the momentum, continuity and heat conservation equations based on marker-in-cell and finite-differences methods:

$$\frac{\partial \sigma'_{ij}}{\partial x_j} - \frac{\partial P}{\partial x_i} + \rho g_i = 0 \tag{1}$$

$$div(\vec{v}) = \frac{\partial v_x}{\partial x} + \frac{\partial v_y}{\partial y} = 0 \tag{2}$$

$$\rho C_P \left(\frac{DT}{Dt}\right) = \frac{\partial}{\partial x_i}\left(k\frac{\partial T}{\partial x_i}\right) + H_a + H_r + H_s \tag{3}$$

where σ'_{ij} is the deviatoric stress tensor; P is the pressure; ρ is the density; g_i is the gravitational acceleration; v_x and v_y are the horizontal and vertical velocity components, respectively; C_P is the isobaric heat capacity; $\frac{DT}{Dt}$ is the substantive time derivative; k is the thermal conductivity coefficient; T is the temperature; H_a, H_r and H_s are adiabatic, radioactive and shear heat production, respectively.

3.2. Rheological model

We consider the plastic and viscous rheology of rocks, which behave like slowly creeping fluids at long time scale. The plastic rheology follows the Drucker-Prager yield criterion at shallow depth and high stress (Ranalli, 1995):

$$\sigma_{yield} = C + P\sin(\varphi)$$

$$\sin(\varphi) = \sin(\varphi_{dry})(1 - \lambda)$$

$$\eta_{plastic} = \frac{\sigma_{yield}}{2\dot{\varepsilon}_{II}} \tag{4}$$

where σ_{yield} is the yield stress; C is the cohesion (i.e., the residual strength at P = 0), φ is the internal friction angle (φ_{dry} stands for dry rocks); λ is the pore fluid pressure factor and $\dot{\varepsilon}_{II}$ is the second invariant of the strain rate.

The viscous rheology takes the form (Ranalli, 1995):

$$\eta_{ductile} = f\,(B*)(\dot{\varepsilon}_{II})^{(1-n)/n}\exp\left(\frac{E_a + PV_a}{nRT}\right) \tag{5}$$

where E_a is activation energy; V_a is activation volume; n is stress exponent; R is the gas constant. f is the scaling factor, which is used to linearly modulate the effective viscosity relative to the reference laboratory data (e.g., Beaumont et al., 2004). This allows us to vary the material strength to approximate the lithospheric strength heterogeneity due to tectonic inheritance and uncertainties in the rheological parameters (e.g., Beaumont et al., 2004). $B*$ is the pre-exponential factor, which is related to material constant (A_D) as follows:

$$B* = AD^{(-1/n)} \tag{6}$$

Finally, the minimum of plastic and ductile viscosities defines the effective viscosity:

$$\eta_{eff} = \min(\eta_{plastic}, \eta_{ductile}) \tag{7}$$

The models incorporate 'wet quartzite' flow law for the upper crust, 'plagioclase An75' for the lower crust, 'dry olivine' for the lithospheric and sub-lithospheric mantle, and 'wet olivine' for the weak zone mantle (Ranalli, 1995). These rheological parameters used in this study are

Table 1
Rheological parameters used in the numerical experiments (Ranalli, 1995).

Material	Flow law	η Pa^n s	n	E_a kJ/mol	V_a J/ (Mpa mol)	sin(φ)	CPa
Sedi.	Wet quartzite	1.97×10^{17}	2.3	154	8	0.15	1×10^6
UCC	Wet quartzite	1.97×10^{17}	2.3	154	12	0.15	1×10^6
LCC	Plagioclase (An75)	4.80×10^{22}	3.2	238	8	0.15	1×10^6
UOC	Wet quartzite	1.97×10^{17}	2.3	154	8	0	1×10^6
LOC	Plagioclase (An75)	4.80×10^{22}	3.2	238	8	0.6	1×10^6
Dry M.	Dry olivine	3.98×10^{16}	3.5	532	8	0.6	1×10^6
Wet M.	Wet olivine	5.01×10^{20}	4.0	470	8	0	1×10^6

Note: Sedi., sediment; UCC, upper continental crust; LCC, lower continental crust; UOC, upper oceanic crust; LCC, lower oceanic crust; Dry M., lithosphere and asthenosphere dry mantle; Wet M., lithosphere and asthenosphere wet mantle.

summarized in Table 1.

3.3. Partial melting model

We take into account partial melting of various lithologies by employing experimentally-constrained solidus ($T_{solidus}$) and liquidus ($T_{liquidus}$) (Table 2). The degree of melt is represented as volumetric melt fraction (M), which is assumed to increase linearly with temperature (Gerya and Yuen, 2003b):

$$M = \begin{cases} 0 & \text{when } T \le T_{solidus} \\ \dfrac{(T - T_{solidus})}{(T_{liquidus} - T_{solidus})} & \text{when } T_{solidus} < T < T_{liquidus} \\ 1 & \text{when } T \ge T_{liquidus} \end{cases} \quad (8)$$

The effective density (ρ_{eff}) of partially molten rocks can be calculated as follows:

$$\rho_{eff} = \rho_{solid} - M(\rho_{solid} - \rho_{molten}) \quad (9)$$

where ρ_{solid} and ρ_{molten} are the densities of the given solid and molten rock, respectively.

3.4. Topography model

The evolution of topography involves the erosion and sedimentation processes, which is calculated at each time-step on the Eulerian grid following the transport equation (Gerya and Yuen, 2003b):

$$\frac{\partial_{y_{es}}}{\partial t} = v_y - v_x \frac{\partial_{y_{es}}}{\partial x} - v_s + v_e \quad (10)$$

where y_{es} is the vertical position of the model surface as a function of the horizontal distance x; v_x and v_y are the horizontal and vertical velocity vector at the surface; v_s and v_e are the sedimentation and erosion rates conforming to the relation:

$v_s = 0$ mm/yr, $v_e = 0.2$ mm/yr when $y_{es} > 4$ km

$v_s = 0.3$ mm/yr, $v_e = 0$ mm/yr when $y_{es} < 1$ km

4. Model setup

The model domain extends 6000 km in the X direction and 820 km in the Y direction, which is resolved by 2001 × 411 Eulerian nodes with a uniform resolution of 3 × 2 km. There are over 12 million Lagrangian markers randomly distributed in the whole domain. This allows us to monitor crustal deformation in detail.

The model setup represents simplified tectonic map of the India-Asia collision zone (Fig. 1a) based on Yin and Harrison (2000). It consists of six tectonic units from left to right, south to north in the model setup (Fig. 2a): Indian plate (2000-km-wide), Tethys Ocean (500-km-wide), proto-southern Asia (1700-km-wide), Tarim basin (800-km-wide), Tian Shan (500-km-wide) and Junggar basin (500-km-wide). It is noteworthy that a narrow Tethys Ocean here is mainly used to facilitate the subsequent subduction of the Indian plate (simple shear), rather than to simulate the whole subduction history of the wide Tethys Ocean. The oceanic crust is composed of 3-km-thick upper crust and 5-km-thick lower crust, overlying 90-km-thick lithospheric mantle (Fig. 2b). The continental lithosphere is divided into three categories with different configurations. The proto-southern Asia is assumed to have a pre-thickened crust composed of 25-km-thick upper crust and 25-km-thick lower crust (Kapp et al., 2005; Murphy et al., 1997), which overlies the 50-km-thick lithospheric mantle. The Tian Shan is assumed to have a 45-km-thick crust composed of 20-km-thick upper crust and 25-km-thick lower crust, which is underlain by 55-km-thick lithospheric mantle (Fig. 2c). The rest of continental domains have the same crustal structure as the Tian Shan, but are underlain by 75-km-thick lithospheric mantle.

All velocity boundary conditions (Fig. 2a) are free slip except the lower boundary, which is permeable to allow the conservation of mass in the computational domain and implies an infinity-like external free slip condition (Burg and Gerya, 2005; Gerya et al., 2008; Li et al., 2016). To simulate the topographical evolution, a 20-km-thick 'sticky air' layer with viscosity of 10^{18} Pa s and density of 1 kg/m^3 (Schmeling et al., 2008; Crameri et al., 2012) is placed at the top of the model as the internal free-surface. The initial geotherm linearly increases from 0 °C at the surface to 1330 °C at the base of the lithosphere beneath all the tectonic units except the Tian Shan, where the temperature first increases linearly from 0 °C at the surface to a given value (e.g., 800 °C for the reference model) at the Moho and then continues to increase with a smaller geothermal gradient to 1330 °C at the lithosphere base. This allows us to test the effect of the thermal state of the Tian Shan crust. Similarly, different Moho temperatures of the proto-southern Asia have also been tested. A mantle adiabat with potential temperature of 1330 °C and adiabatic gradient of 0.5 °C/km is used for the sub-lithospheric mantle. The thermal boundary conditions are illustrated in Fig. 2a. The temperature is set constant (0 °C) for the top boundary and the side boundaries are insulating (no horizontal heat flux). An infinity-like external constant temperature condition is used for the lower boundary (Burg and Gerya, 2005).

To drive the whole subduction-collision system, a constant convergence rate is applied at the left side of the model (X = 1500 km). The convergence rate in our models is based on estimates of Cenozoic shortening rates across the Asian continent, north of the Himalayan fold-thrust belt. Thus, our model involves shortening rates that are less than the India-Asia convergence rate (Molnar and Stock, 2009), which we justify because our model excludes any out-of-plane motion related to lateral extrusion along large-scale strike-slip faults (e.g., Tapponnier et al., 1982; Armijo et al., 1986, 1989). For comparison purposes, we refer to the left and right sides of the model as south and north in the rest of the paper. The West Kunlun range is defined as 150 km wide forming the northern boundary of the Tibetan plateau. The Tian Shan is sandwiched between the Tarim and Junggar basins on low topography.

Table 2
Thermal properties used in the numerical experiments.

Material	ρkg/ m^3	k W/(m k)	$T_{solidus}$ K)	$T_{liquidus}$ K	Q_l kJ/kg	Hr μW/m^3
Sedi.	2600 (solid) 2400 (molten)	[0.64 + 807/(T + 77)]	889 + 17,900 / (P + 54) + 20,200 / $(P + 54)^2$ at P < 1200 MPa 831 + 0.06P at P > 1200 MPa	1262 + 0.09P	300	1.5
UCC	2700 (solid) 2400 (molten)	[0.64 + 807/(T + 77)]	889 + 17,900 / (P + 54) + 20,200 / $(P + 54)^2$ at P < 1200 MPa 831 + 0.06P at P > 1200 MPa	1262 + 0.09P	300	1.2
LCC	2800 (solid) 2400 (molten)	[1.18 + 474/(T + 77)]	1327.15 + 0.0906P	1423 + 0.105P	380	0.4
UOC	3000 (solid) 2900 (molten)	[1.18 + 474/(T + 77)]	1327.15 + 0.0906P	1423 + 0.105P	380	0.25
LOC	3000 (solid) 2900 (molten)	[1.18 + 474/(T + 77)]	1327.15 + 0.0906P	1423 + 0.105P	380	0.25
Dry M.	3300 (solid) 2900 (molten)	[0.73 + 1293/(T + 77)] × (1 + 0.00004P)	1394 + 0.132899P − 0.000005104P^2 at P < 10,000 MPa 2212 + 0.030819(P − 10000) at P > 10,000 MPa	2073 + 0.114P	400	0.022
Wet M.	3200 (solid) 2900 (molten)	[1.18 + 474/(T + 77)]	1240 + 49,800 / (P + 323) at P < 2400 MPa 1266–0.0118P + 0.0000035P^2 at P > 2400 MPa	2073 + 0.114P	400	0.022
References	[a, b]	[c, d]	[e, f, g, h, i]	[g]	[a, b]	[b]

[a] Bittner and Schmeling (1995).
[b] Turcotte and Schubert (2002).
[c] Clauser and Huenges (1995).
[d] Hofmeister (1999).
[e] Johannes (1985).
[f] Hess (1989).
[g] Schmidt and Poli (1998).
[h] Hirschmann (2000).
[i] Poli and Schmidt (2002).

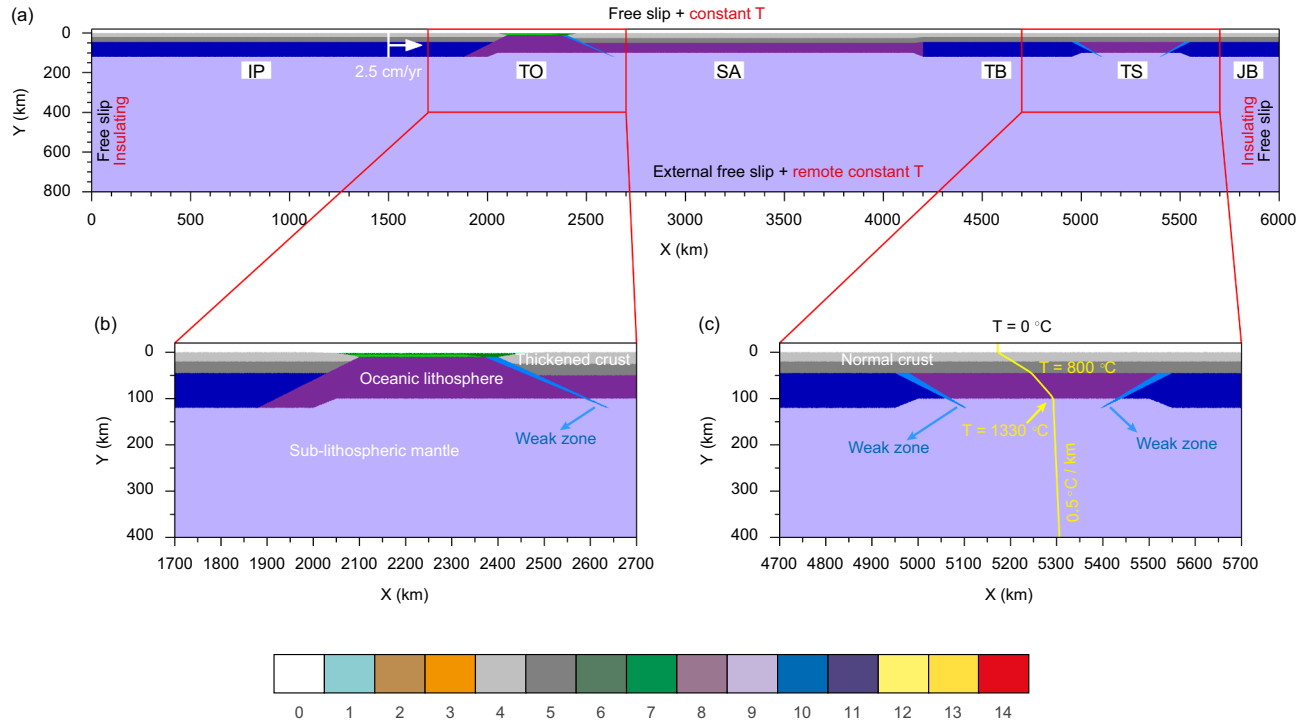

Fig. 2. Model setup. (a) Initial model configuration and thermal-mechanical boundary conditions. White arrow represents the convergence rate, which is imposed at X = 1500 km. (b) and (c) Zoomed domains corresponding to red rectangles in (a). Yellow line indicates the initial temperature profile in the Tian Shan. Abbreviations: IP: Indian plate; TO: Tethys Ocean; SA, proto-southern Asia; TB, Tarim basin; TS, Tian Shan; JB, Junggar basin. The color code shows different rock types, with: 0-air; 1-water; 2 and 3-sediment; 4-upper continental crust; 5-lower continental crust; 6-upper oceanic crust; 7-lower oceanic crust; 8 and 11-lithospheric mantle; 9-athenospheric mantle; 10-weak zone mantle; 12 and 13-partially molten sediment; 14, partially molten continental crust.

5. Results

We performed 20 numerical experiments to investigate the effects of convergence rate as well as thermal state of the proto-southern Asia and the Tian Shan on stress transfer and intraplate orogeny. All the models show similar episodes of evolution, including (1) subduction of the Tethys Ocean, (2) continental collision, and (3) intraplate orogeny. The variations in model parameters alter the deformation style and associated topography expression, but the above-mentioned three episodes hold for all the models.

The reference model involved the following parameters. (1) Convergence rate (V) was set at 2.5 cm/yr, which is in agreement with the estimate of Cenozoic shortening rate of Asian plate at present (Guillot et al., 2003). (2) The Moho temperatures of the proto-southern Asia (T_{MP}) and the Tian Shan (T_{MT}) were set at 665 °C and 800 °C respectively, and the hot Moho underneath the Tian Shan is supported by electrical conductivity of xenoliths study that suggested a Moho temperature of 850 °C prior to shortening strain (Bagdassarov et al., 2011). (3) The strength of lithospheric mantle of the Indian, Tarim and Junggar blocks was adopted to be two times stronger than that of the Asian and Tian Shan blocks (i.e., f = 2).

5.1. Reference model

Fig. 3 shows selected snapshots of the evolution of the reference model. At the initial stage, the Tethys Ocean subducts underneath the proto-southern Asia (Fig. 3a). A supra-subduction basin forms on the continental margin of the upper plate, which accommodates the subsidence of the upper plate's margin. The boundary convergence has little impact on the deformation of the upper plate's interior, where the horizontal deviatoric stress is low and the strain rate is generally slow. The proto-southern Asian and Tian Shan blocks experience a transient extensional state due to their hot thermal states.

As convergence continues, slab subduction is replaced by continent collision. The pro-continent coupled to the oceanic plate is dragged down to the depth of 200 km where the necking and breakoff of oceanic lithosphere occur after ~25.4 Myr of convergence (Fig. 3b). When the slab experiences complete breakoff, the India-Asia convergence would no longer be consumed by slab subduction but rather by the deformation in the mantle wedge and subsequent far-field transfer of compressional stress. The deformation of the upper plate becomes faster relative to the initial stage, and significant strain localizes at the boundaries between the strong and weak blocks, e.g., the south and north slopes of the Tian Shan block (see the second invariant of strain rate field).

Continuous convergence finally causes intraplate orogeny. After 55.8 Myr of convergence, the horizontal stress in response to the India-Asia collision is transferred further northward by the rigid Tarim basin triggering intraplate orogeny (Fig. 3c). The continued convergence thickens the crust of the proto-southern Asia at the margin and causes the formation of the Tibetan plateau (Fig. 4a, b). The cold Tarim basin behaves as a rigid block and transfers stress to the Tian Shan. This leads to strong crust-level fold-and-thrust deformation with a wavelength of ~60 km within the Tian Shan. As a consequence, the strain concentrates on both the weak Tian Shan and West Kunlun range, while the strong Tarim basin is less deformed.

The topographic expression in response to the above-mentioned geodynamic processes is illustrated in Fig. 4c–e. The stage of Tethys Ocean subduction is characterized by the formation of deep trench. After ~10 Myr of convergence, the topography reaches the height of 1–2 km due to the extrusion of accretionary wedge, which marks the closure of the Tethys Ocean and the beginning of the continental collision stage (Fig. 4c). In response to the slab breakoff and resultant dynamic rebound, an abrupt topographic uplift takes place on the subducted plate, which further results in the disappearance of the trench. Subsequently, the Tian Shan and West Kunlun range uplifts after

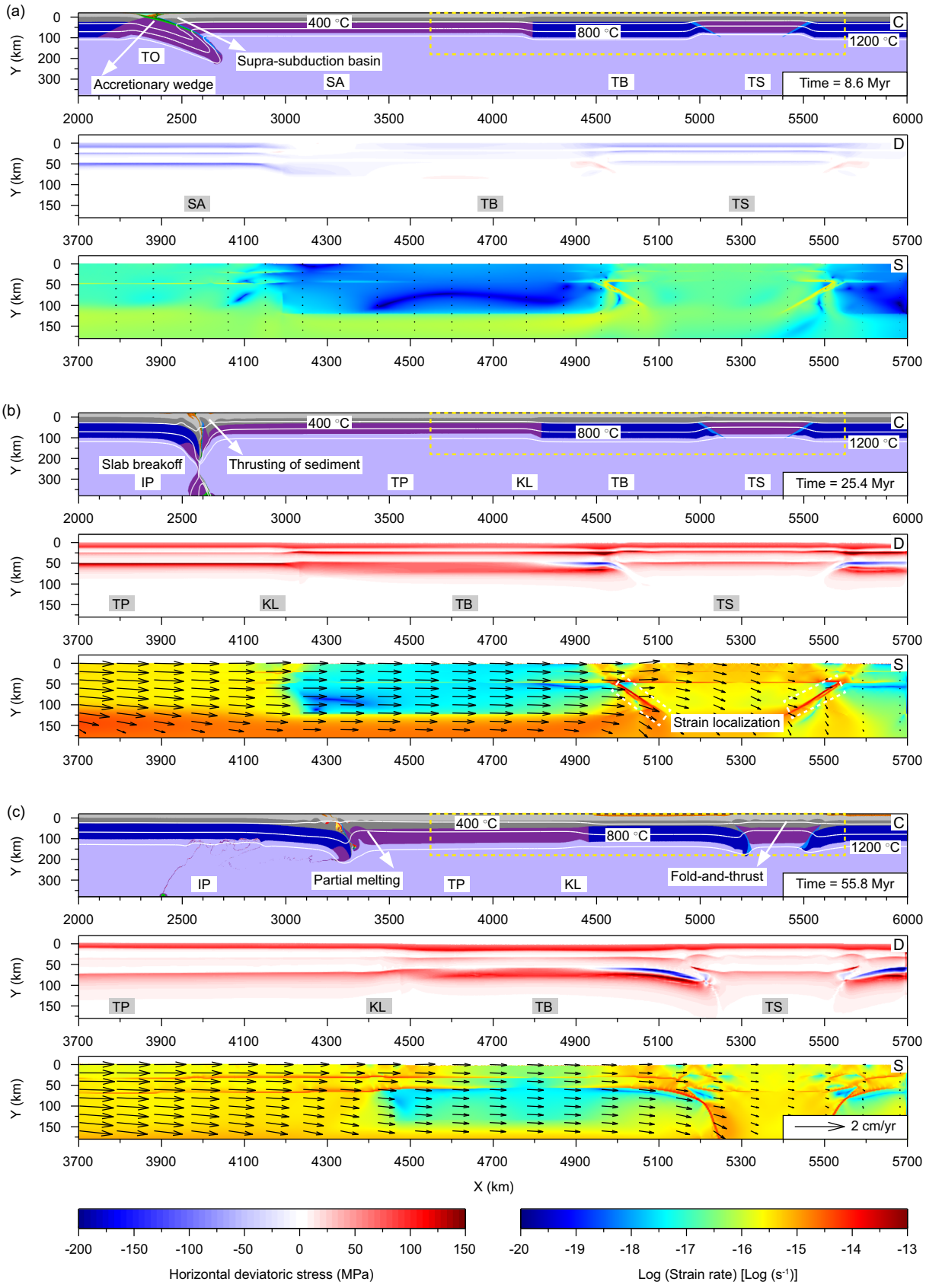

Fig. 3. Temporal evolution of the reference model (Model a) at three different stages: (a) subduction of Tethys Ocean, (b) continental collision and (c) intraplate orogeny. At the initial stage, the boundary convergence was consumed by slab subduction. After the slab breakoff, the India-Asia convergence is transferred into the upper plate's interior, resulting in the deformation of intraplate orogens. The composition fields illustrate deformation features at each stage, with white lines representing the isotherms with a 400 °C increment. The horizontal deviatoric stress fields demonstrate a progressive accumulation process (positive on compression). The strain rate distribution fields present that strain is localized after slab breakoff, with black arrows representing the velocity fields. Abbreviations: C, composition field; D, horizontal deviatoric stress; S, strain rate distribution; TP, Tibetan plateau; KL, West Kunlun; rest are the same as those in Fig. 2.

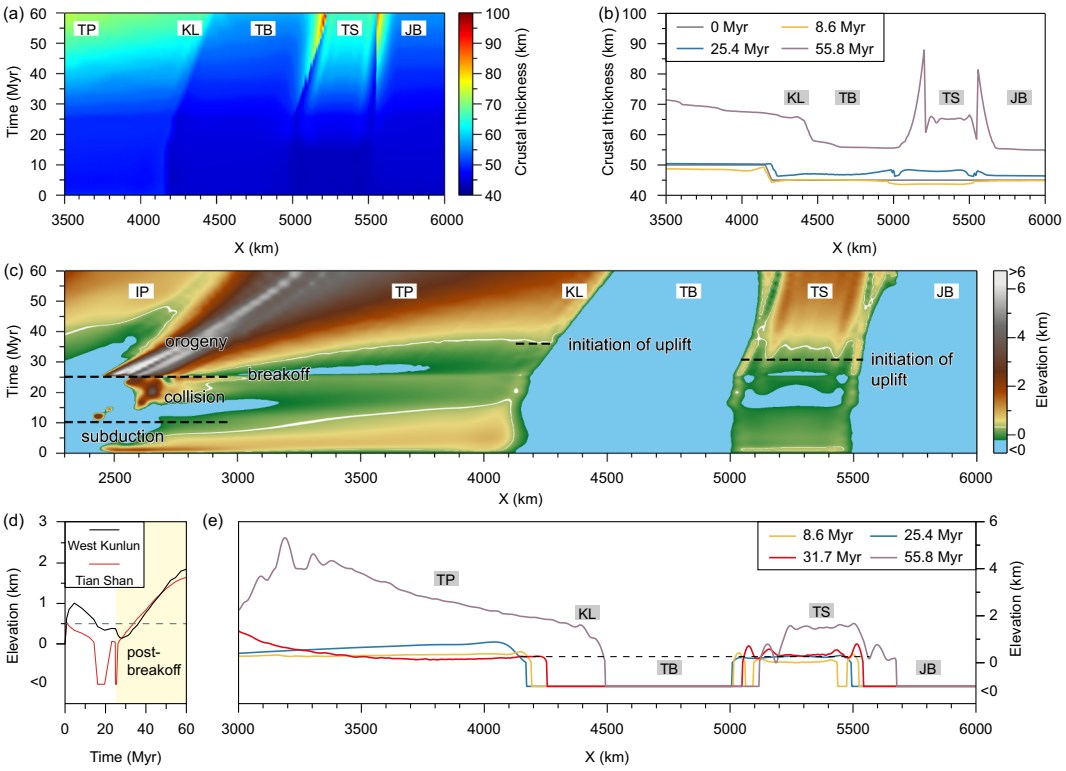

Fig. 4. Crustal thickness and topography evolution of the reference model. (a) Crustal thickness evolution with time. (b) Crustal thickness distribution at 0, 8.6, 25.4, and 55.8 Myr, respectively. (c) Topography evolution with time. The time when elevation reaches 500 m represents the initiation of uplift (white-colored contour line), and in this case Tian Shan uplifted earlier than that of West Kunlun range, demonstrating a diachronous rise pattern. (d) Topographic profiles of the Tian Shan and the West Kunlun. Light yellow-colored region represents post-breakoff stage. The result illustrates that elevation of the Tian Shan was higher than that of West Kunlun range during 28–45 Myr of modeling time, and that the Tian Shan reaches the elevation of 500 m earlier than the West Kunlun range. The negative elevation occurs due to the limitation of simplified erosion and sedimentation processes and has been uniformly set to fixed values. (e) Snapshots of topography distribution at 8.6, 25.4, 31.7 and 55.8 Myr, respectively. Abbreviations are the same as those in Fig. 3.

~31 Myr and ~36 Myr of convergence respectively, presenting the out-of-sequence uplift. When analyzing the uplift sequence of West Kunlun range and Tian Shan after India-Asia collision, a reference elevation of 500 m (white-colored contour line in the topographic elevation plots) was adopted to define the uplift caused by the collision because the thrust belts had experienced slow cooling rates of ~ > 0.01–0.02 mm/yr prior to the initiation of rapid uplift (De Grave et al., 2011; Dai et al., 2013; Wang et al., 2016, 2017; Cheng et al., 2018). Finally, the topographic map presents an overall uplift pattern across the Tibetan plateau and the Tian Shan, where the elevation reached 2–3 km.

5.2. Effects of convergence rate

Since the Indian plate indented against the Asian plate with decelerating rates during its northeastward drifting (Molnar and Stock, 2009), the far-field effects under different shortening rates should be tested. This group of models (Models a, b, c in Table 3) was designed to examine the influence of convergence rate on the far-field stress transfer of continental collision. A lower and a higher convergence rates were set to 1 cm/yr (Model b) and 5 cm/yr (Model c) respectively, relative to the reference model (Model a, V = 2.5 cm/yr). At the same amount of convergence length (Figs. 5, 6), the results are comparable to that of the reference model, with the differences being the deformation style and topographical evolution of intraplate thrust belts.

At a low convergence rate (V = 1 cm/yr, Model b), the rigid Tarim and Junggar blocks tend to subduct into the deep asthenospheric mantle beneath the Tian Shan (Fig. 5a). In this case, the stress transferred from the south is dominantly consumed by this bi-directional subduction, rather than deforming the Tian Shan's crust and driving topographic uplift. Consequently, the topographic peak of the Tian Shan is lower than 1 km and initiation of uplift is much later than in the West Kunlun range (Fig. 6a). The high elevation of the West Kunlun range propagates northward to the southern margin of the Tarim basin, creating a gradual topographic slope between them (Fig. 6a).

Table 3
Parameters and results of the numerical experiments.

Model name	V cm/yr	T_{MT} °C	T_{Mp} °C	Figures	Comments
Model a	2.5	800	665	3 and 4	Reference model
Model b	1	800	665	5 and 6	Sequential rise
Model c	5	800	665		Diachronous rise
Model d	2.5	600	665	8 and 9	Failed rise
Model e	2.5	700	665		Sequential rise
Model f	2.5	900	665		Diachronous rise
Model g	2.5	800	600	10	Diachronous rise
Model h	2.5	800	800		Sequential rise

V, convergence rate; T_{MT}, initial Moho temperature of the Tian Shan; T_{MP}, initial Moho temperature of the proto-southern Asia.

At the medium (V = 2.5 cm/yr) and high (V = 5 cm/yr) convergence rates, boundary stress is transferred northward more efficiently. This leads to more pronounced crustal buckling and narrower ranges within the Tian Shan block (Fig. 5b, c). As a consequence, strain is significantly strengthened in both the Tian Shan and the West Kunlun range relative to that at a slow convergence rate (Fig. 5a). In both cases, the Tian Shan experienced an earlier uplift than the West Kunlun range (Fig. 6b, c). A high convergence rate enlarges the time lag. For instance, when V = 5 cm/yr, the Tian Shan uplifts after ~13 Myr of convergence, while the elevation of the northern margin of Tibetan plateau is below sea level until ~26 Myr (Fig. 6c).

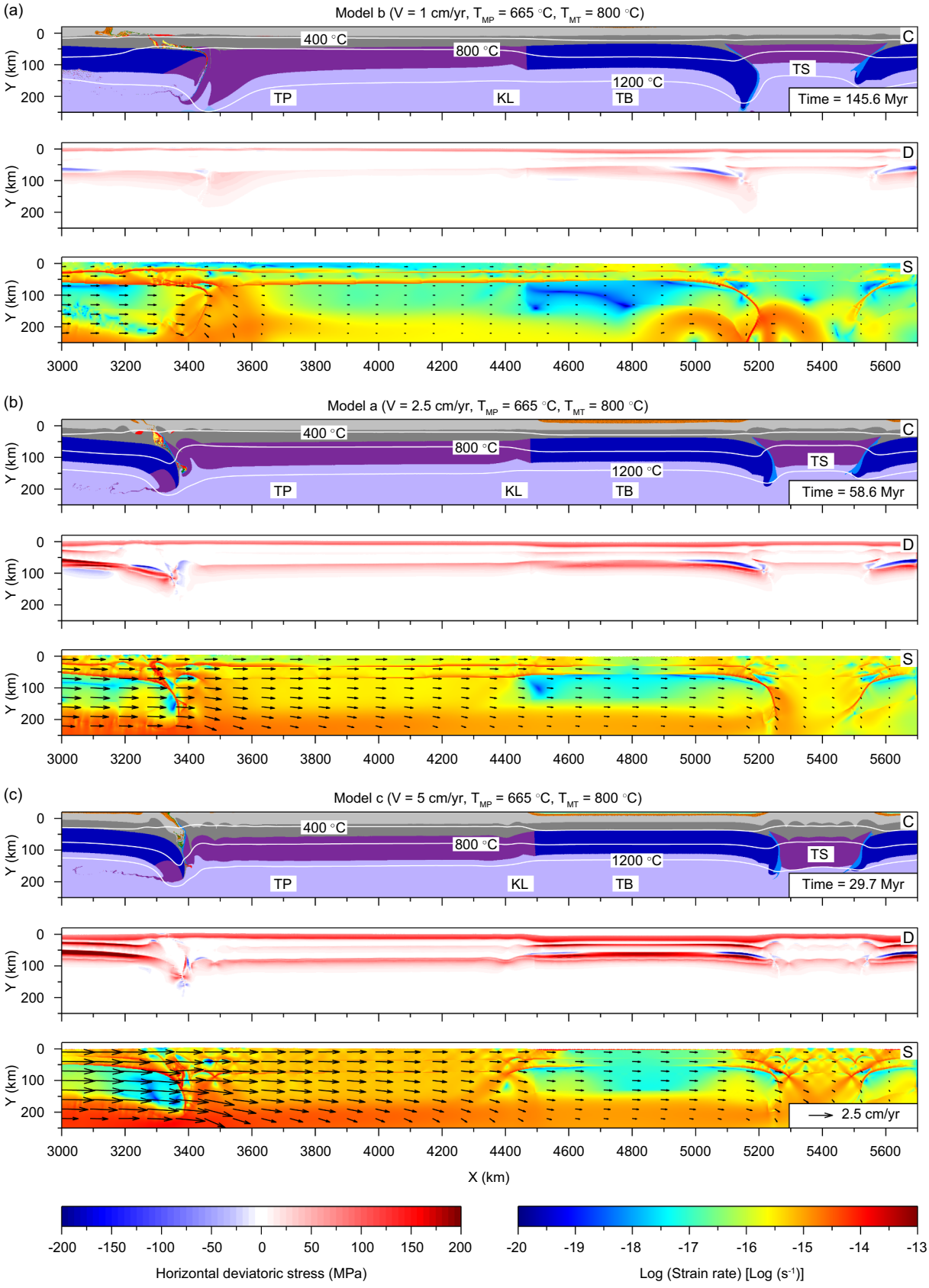

Fig. 5. Results with respect to different convergence rates. (a) Model b at 1 cm/yr. (b) Model a at 2.5 cm/yr. (c) Model c at 5 cm/yr. They are compared at the same amount of convergence length of ~1500 km. As the convergence rate increases, the boundary stress is more efficiently transferred into the upper plate's interior. This leads to more pronounced crustal buckling and narrower orogens within the Tian Shan block. As a consequence, strain is significantly strengthened in the Tian Shan and the West Kunlun range. White line represents the isotherms for increments of 400 °C. Black arrows represent the velocity fields. Abbreviations: V, convergence rate; T_{MP}, the Moho temperature of the proto-southern Asia; T_{MT}, the Moho temperature of the Tian Shan; rest are the same as those in Fig. 3.

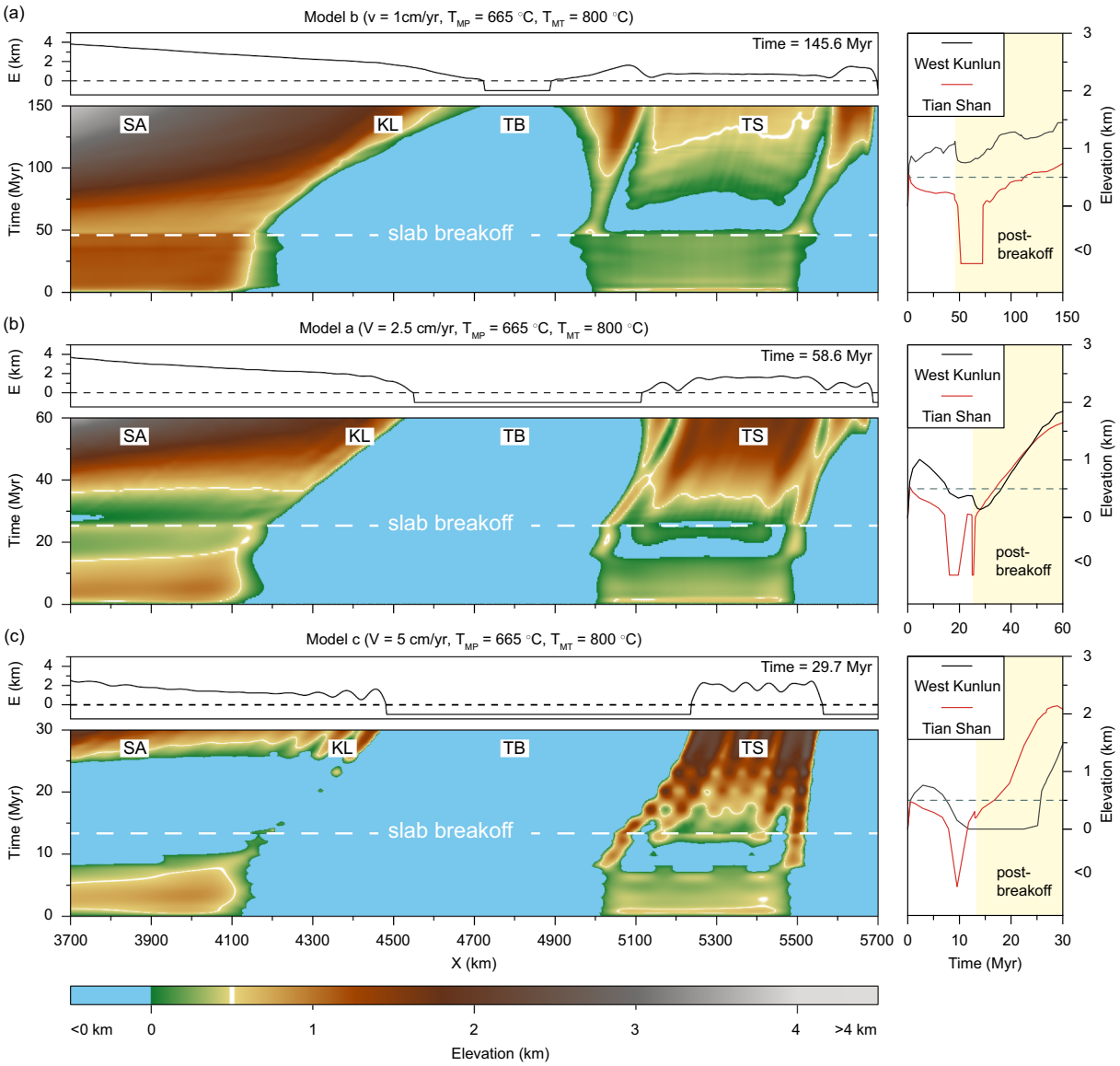

Fig. 6. Topographic evolution of the models with different convergence rates. (a) Model b at 1 cm/yr. (b) Model a at 2.5 cm/yr. (c) Model c at 5 cm/yr. In each case, on the left side, the top graph shows topography distribution at the end of modeling, while the bottom figure illustrates topography evolution with time; topographic profiles of the Tian Shan and West Kunlun range are presented on the right side (light yellow-colored region represents post-breakoff stage). Under a convergence rate of 1 cm/yr (Model b), the West Kunlun range uplifts earlier than the Tian Shan (reached elevation of 500 m). Under a convergence rate of 2.5 cm/yr (Model a), the Tian Shan uplifts earlier than the West Kunlun range by ~5 Myr (diachronous rise pattern occurs). When convergence rate reaches 5 cm/yr (Model c), diachronous rise pattern remains and the Tian Shan uplifts earlier than the West Kunlun range by ~13 Myr. Abbreviations are the same as those in Fig. 3.

In general, the convergence rate facilitates the build-up of topography (Fig. 6). Faster convergence rate results in earlier and higher uplift of the Tian Shan, which even precedes the uplift of the West Kunlun range at a convergence rate of > 2.5 cm/yr.

5.3. Effects of thermal heterogeneity

The lithospheric thermal state strongly affects the rheological strength (Burov and Watts, 2006; Gueydan et al., 2008; Schmalholz et al., 2009). Thus, we designed two groups of models to test the lithospheric thermal state contrast between the strong and weak blocks in the upper plate deformation by varying the Moho temperature of both the Tian Shan (T_{MT} = 600, 700 and 900 °C) and proto-southern Asia (T_{MP} = 600 and 800 °C), respectively. Results show that a high initial Moho temperature dramatically reduces the viscosity of the lower crust and upper lithospheric mantle (Fig. 7a, b).

A group of models (Models d, e, f in Table 3) with different Moho temperatures of the Tian Shan shows similar composition evolutions to the reference model except the extent of lithospheric deformation during intraplate orogeny (Fig. 8). As the initial Moho temperature increases, the strain is more easily to be transferred and concentrated on the rheologically weaker Tian Shan through lithospheric shortening and crustal buckling. The much intensive deformation domains are illustrated as smaller values in the horizontal deviatoric stress fields (i.e., white or light reddish color in the horizontal deviatoric stress chart of Fig. 8).

The thermal state of the Tian Shan plays a decisive role in the intraplate orogeny that is characterized by various topographical buildups. At a low Moho temperature of 600 °C (T_{MT} = 600 °C), the topographic evolution shows no obvious uplift of the Tian Shan, in which the elevation is always below sea level (Fig. 9a). When the Moho temperature increases to 700 °C (T_{MT} = 700 °C), the Tian Shan experiences a period of low elevation and then uplifts to the same value as the northern Tibetan plateau (i.e. the West Kunlun range, Fig. 9b). The

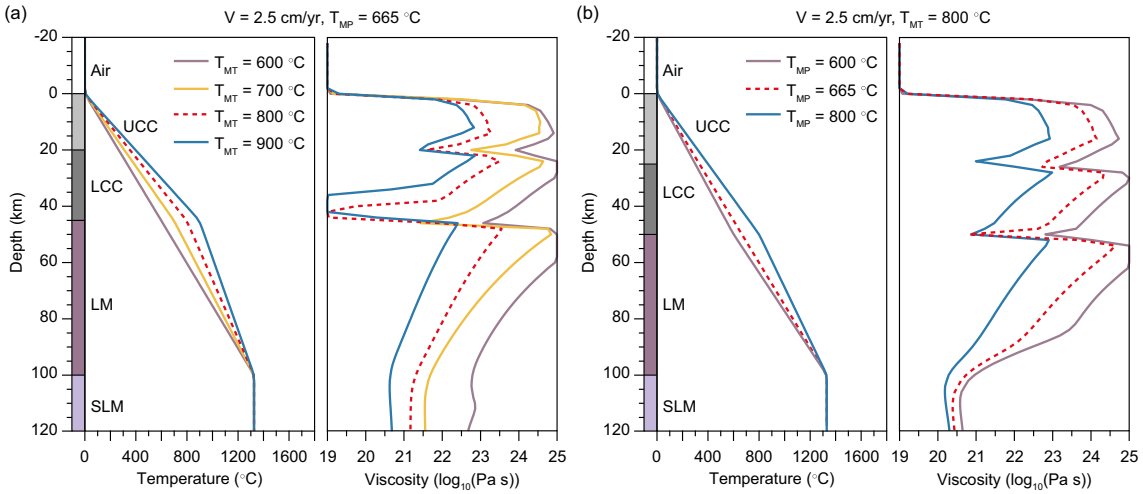

Fig. 7. Initial temperature profiles and viscosity profiles at the very beginning with respect to the different lithospheric temperature structures under (a) the Tian Shan and (b) the proto-southern Asia. Two groups of models were tested by varying the Moho temperature of both the Tian Shan (T_{MT} = 600, 700, 800 and 900 °C) and proto-southern Asia (T_{MP} = 600, 665 and 800 °C). A high initial Moho temperature dramatically reduces the viscosity of the lower crust and upper lithospheric mantle. The red dotted line represents the reference model. Abbreviations: UCC, upper continental crust; LCC, lower continental crust; LM, lithospheric mantle; SLM, sub-lithospheric mantle.

uplift time of the Tian Shan after ~40 Myr of convergence lags behind that of the West Kunlun range after ~34 Myr of convergence (Fig. 9b). When the Moho temperature is up to 900 °C (T_{MT} = 900 °C), the topography of the Tian Shan is rapidly built up and finally reaches the peak value that is greater than those in other models (Fig. 9c). It is noteworthy that the uplift of the West Kunlun range lags behind that of the Tian Shan under this condition, which may be due to stronger resistance of the Tibetan lithosphere.

The thermal state of the West Kunlun range also largely affects intraplate orogeny (Models g, h in Table 3). Since the models return results that are comparable to those of the reference model, only the topographic evolution graphs are illustrated here. Relative to the case of reference model (T_{MP} = 665 °C), a lower Moho temperature of the proto-southern Asia (T_{MP} = 600 °C) leads to an earlier uplift in the Tian Shan than in the West Kunlun range (Figs. 6b, 10a). When the Moho temperature of the proto-southern Asia was set higher to 800 °C, the West Kunlun range involves earlier and higher uplift, and uplift of the Tian Shan lags behind that of the West Kunlun range for ~9 Myr (Fig. 10b).

6. Discussion

In this section, we first compare our model results to the geological and geophysical observations in the Tibetan orogen-Tian Shan thrust belt system. We then discuss the far-field effect of India-Asia collision on intraplate orogeny and present the possible mechanism to interpret the diachronous topographic rise between the Tian Shan and the West Kunlun range. Finally, we discuss the limitations in the numerical modeling.

6.1. Comparison with geological or geophysical observations

Several first-order characteristics observed in the models are comparable to regional geological or geophysical observations. First, modeling (Fig. 4e) reproduces a topographic pattern that is characterized by a basin sandwiched by two thrust belts, where fold-thrust systems are topographically higher and surround a relatively undeformed basin. This is coincident with the present topography with a high-low-high feature on the profile (Fig. 1b). Second, modeled crustal thickness alternates between relatively thicker and thinner crustal blocks (Fig. 4b), which agrees with geophysical observations for variable crustal thickness within the Tibetan orogen-Tian Shan thrust belt system (Nelson et al., 1996; Kosarev et al., 1999; Kumar et al., 2005; Zhang et al., 2011; Tunini et al., 2016). Furthermore, the abrupt Moho offsets near the margin of the Tian Shan (Fig. 4b) have been supported by the evidence that lithospheric mantle of both the Tarim and the Junggar basins subducted bilaterally beneath the Tian Shan (Avouac et al., 1993; Kao et al., 2001; Gao et al., 2013).

6.2. Intraplate orogeny pattern

All results are compiled according to the major parameters adopted in the modeling, which can be grouped into three end-member patterns with regard to the sequence of intraplate orogeny (Fig. 11). In the failed-rise pattern, insufficient amount of stress is transferred northward to cause the uplift of the Tian Shan. In the sequential-rise pattern, sufficient stress is transferred northward, leading to the earlier uplift of the West Kunlun range at the south and later uplift of the Tian Shan at the north. In the diachronous-rise pattern, the uplift of the Tian Shan at the north is earlier than that of the West Kunlun range at the south.

The model results indicate that the intraplate orogeny pattern may be controlled by the contrast in the Moho temperature between the proto-southern Asian and the Tian Shan (Fig. 11a). In fact, when the Moho temperature of proto-southern Asia is higher than that of the Tian Shan, it is not likely for the Tian Shan to uplift. In this case, the stress produced by convergence is preferentially accommodated by lithospheric deformation within Tibet, rather than transferred northward to induce significant far-field effects. In contrast, when the Moho temperature of the Tian Shan is higher than that of the proto-southern Asia by > 100 °C, diachronous rise appears between the two thrust belts, in the case of which the deformation in the weaker Tian Shan responses quicker to the effects by far-field stress transfer and the time lag increases as the contrast in temperature increases. When the Moho temperature of the Tian Shan is higher than that of the proto-southern Asia by < 100 °C, the intraplate orogeny presents a sequential-rise pattern. In this case, the West Kunlun range and the Tian Shan uplift sequentially in response to the far-field stress transfer. In general, the stress induced by plate convergence prefers to be transferred firstly to the block that is hotter and thus weaker than others, rather than to be concentrated firstly to a neighboring block and then transferred to a further block.

Faster convergence rates amplify the effects caused by the difference

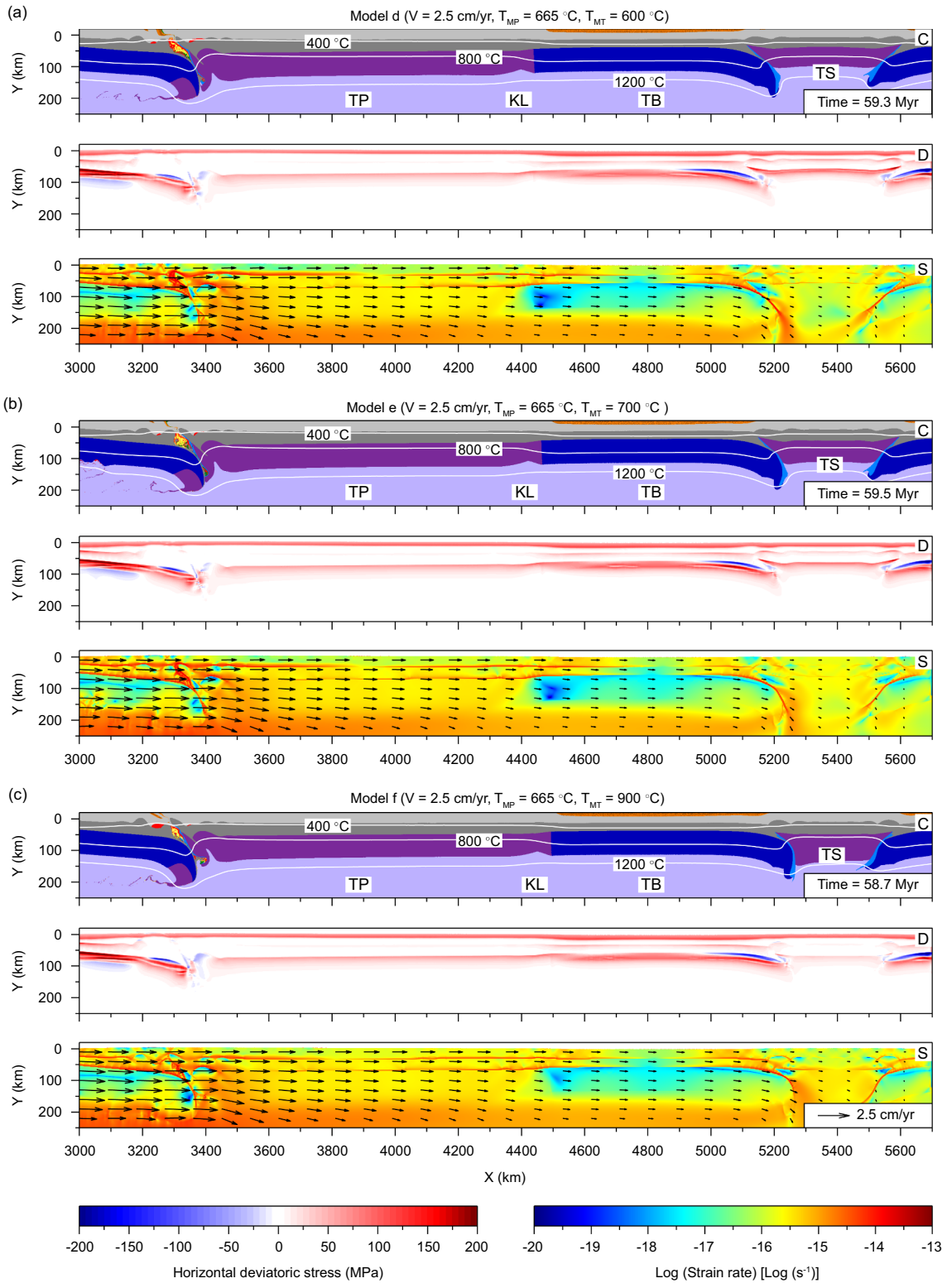

Fig. 8. Results with respect to different Tian Shan lithospheric temperature structures. (a) Model d at 600 °C; (b) Model e at 700 °C; (c) Model f at 900 °C. They are compared at the end of modeling. As the initial Moho temperature of Tian Shan increases, the strain is more easily to be transferred and concentrated on the rheologically weaker Tian Shan through lithospheric shortening and crustal buckling. White line represents the isotherms with an increment of 400 °C. Black arrows represent the velocity fields. Abbreviations are the same as those in Fig. 3.

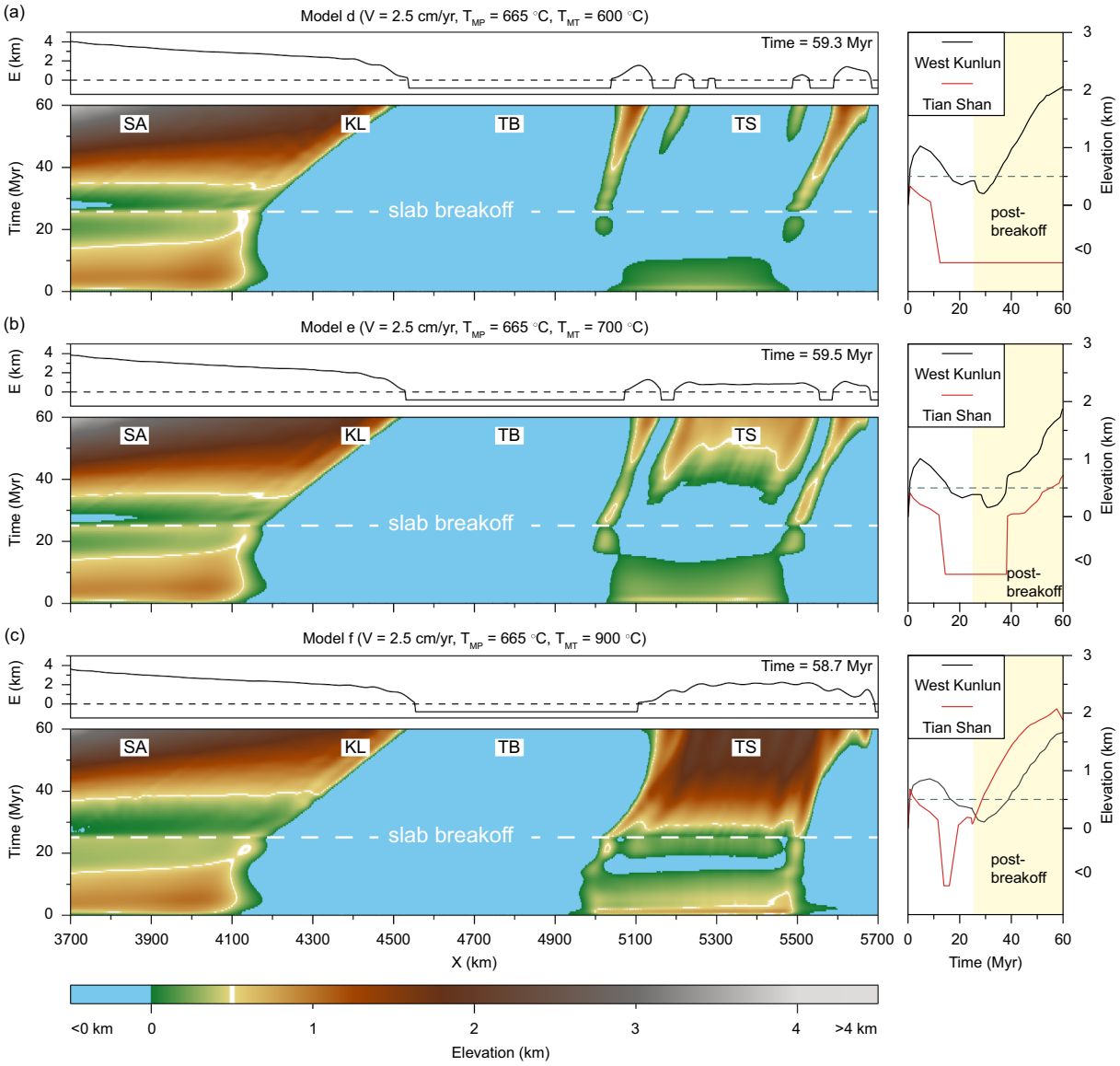

Fig. 9. Topographic evolution of the models with different Moho temperatures of Tian Shan at (a) 600 °C in Model d, (b) 700 °C in Model e and (c) 900 °C in Model f. In each case, on the left side, the top graph shows topography distribution at the end of modeling, while the bottom figure illustrates topography evolution with time; topographic profiles of the Tian Shan and West Kunlun range are presented on the right side (light yellow-colored region represents post-breakoff stage). Response on topographic rise of the Tian Shan depends on its Moho temperature when the proto-southern Asia has a fixed Moho temperature of 665 °C, i.e., no response under a low temperature (Model d, T_{MT} = 600 °C), slow response (later than that of West Kunlun range) under a higher temperature (Model e, T_{MT} = 700 °C), or quick response under an even higher temperature (Model e, T_{MT} = 900 °C), which is earlier than that of the West Kunlun range by ~8 Myr.

in the Moho temperature (Fig. 11b), especially in the condition when the Moho temperature of the proto-southern Asia is lower than that of the Tian Shan. When convergence rate increases from 1 cm/yr to 5 cm/yr, sequential rise between the West Kunlun range and the Tian Shan changes to the diachronous rise pattern. That is to say, faster convergence between the India and Asia plates is beneficial for the stress to be transferred through the rigid Tarim basin.

6.3. Diachronous rise of orogeny

How stress is transferred across the Tibetan plateau has long been debated (Dewey and Burke, 1973; Molnar and Tapponnier, 1975; England and McKenzie, 1982; Avouac et al., 1993; Royden, 1996; Tapponnier et al., 2001; Dayem et al., 2009), but observations of deformation within the Asian continent suggest that residual stress has propagated northward across the relatively rigid Tarim and Qaidam basins (Molnar and Tapponnier, 1975, 1978; Windley et al., 1990; Avouac et al., 1993; Neil and Houseman, 1997; Sobel et al., 2006; Vassallo et al., 2007; Glorie et al., 2011). If this propagation involved a steady northward progression, the uplift of the West Kunlun range is predicted to have occurred earlier than that of the Tian Shan because it is closer to the collision front (Fig. 1a). However, this hypothesis conflicts with the timing of intraplate orogeny constrained by both stratigraphic records and thermochronological data, which suggest that the deformation in the Tian Shan preceded that in the West Kunlun range by ~2–3 Myr (see summary in the Section 2). Similarly, the Qilian Shan uplifted millions to tens of millions of years prior to the East Kunlun range, which is at odds with a northward growing orogen. It is therefore critical to explore the mechanism producing this diachronous pattern of the intraplate orogeny under the framework of far-field stress transfer model.

One possible explanation for out-of-sequence orogeny relies on focused precipitation and correlated surface processes, as suggested by research in the Himalayas (e.g., Hodges et al., 2004). However, most of

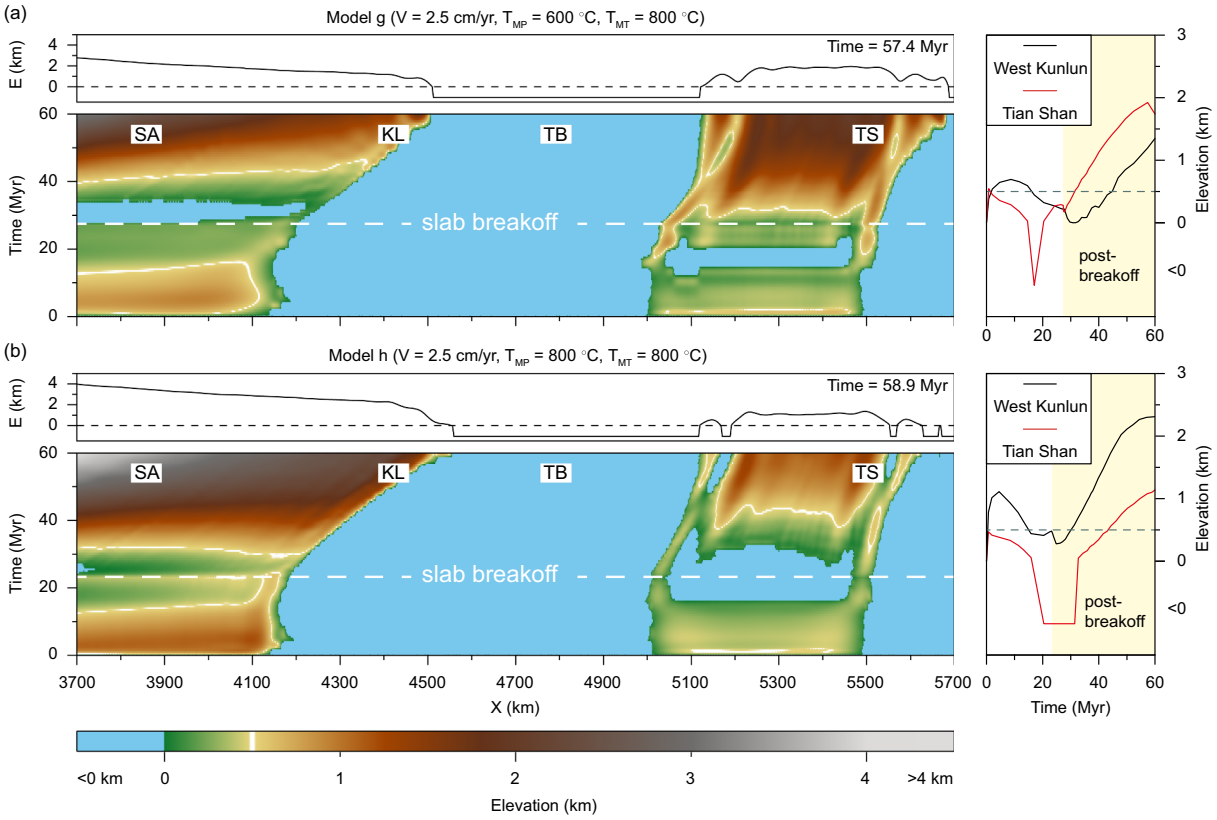

Fig. 10. Topographic evolution of the models with different Moho temperatures of proto-southern Asia at (a) 600 °C in Model g and (b) 800 °C in Model h. In each case, on the left side, the top graph shows topography distribution at the end of modeling, while the bottom figure illustrates topography evolution with time; topographic profiles of the Tian Shan and West Kunlun range are presented on the right side (light yellow-colored region represents post-breakoff stage). Sequence on topographic response between the West Kunlun range and the Tian Shan depends on the Moho temperature of the West Kunlun (T_{MP}) when the Tian Shan has a fixed Moho temperature of 800 °C. When T_{MP} = 600 °C (Model g), topographic response of the Tian Shan occurs earlier than the West Kunlun range (diachronous rise) by ~15 Myr, while when T_{MP} = 800 °C (Model h), topographic response of the Tian Shan occurs later than that of the West Kunlun range (sequential rise). Abbreviations are the same as those in Fig. 3.

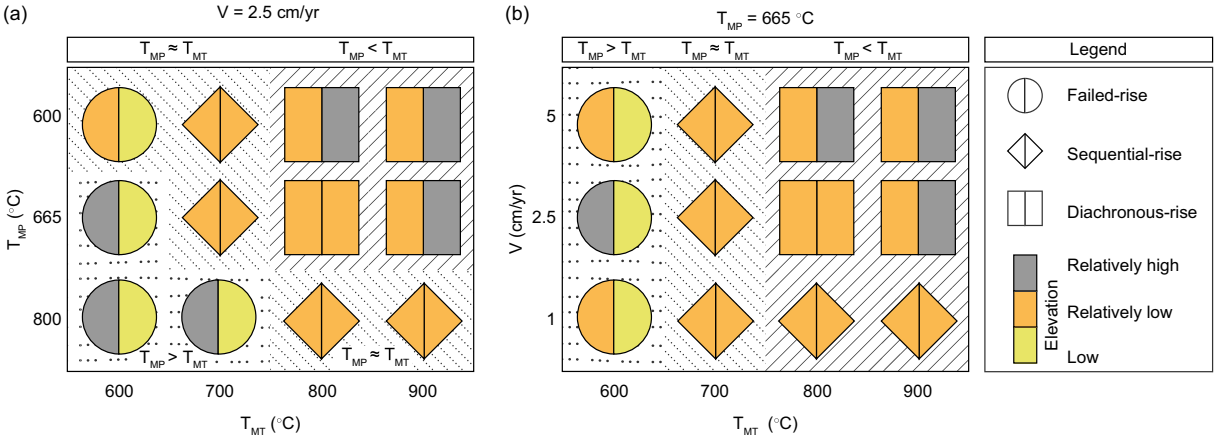

Fig. 11. (a) Intraplate orogeny pattern is depended on the comparison in Moho temperature between the proto-southern Asia (T_{MP}) and the Tian Shan (T_{MT}). When T_{MP} > T_{MT}, the Tian Shan shows failed-rise pattern. When T_{MP} < T_{MT} but the difference is < 100 °C, the intraplate orogeny presents a sequential-rise pattern. In contrast, when T_{MP} < T_{MT} with a difference of > 100 °C, diachronous rise pattern appears. A larger temperature contrast results in a bigger difference in final topography. (b) The convergence rate at the boundary affects the far-field stress transfer. Especially, when T_{MP} < T_{MT}, a higher convergence rate leads to a quicker response and larger amount of rise in topography of Tian Shan, giving rise to a change in orogeny pattern from sequential rise to diachronous rise. Shapes represent different intraplate orogeny patterns: circular for failed-rise pattern, rhombus for sequential-rise pattern and rectangle for diachronous-rise pattern. Colors represent the relative elevation between the West Kunlun range (left) and the Tian Shan (right).

the thrust systems far away from the Himalayan front did not experience enhanced precipitation, and the scale of the Himalaya is an order of magnitude greater than the deformational systems on the plateau (e.g., Zuza et al., 2019) and thus these analogies may not be useful. Another interpretation suggests out-of-sequence orogeny is related to lithospheric buckling over the plateau scale as indicated by analogue modeling (Burg et al., 1994). However, laterally constant material properties and viscosity of each layer assumed in these models seem contrast with observations revealing north-south lithospheric heterogeneity of the Tibet plateau and surrounding regions (Molnar and Tapponnier, 1975, 1978; England and Houseman, 1985, 1986; Roecker et al., 1993; Yin and Harrison, 2000; Zhu et al., 2013).

Alternatively, our results reasonably explain diachronous uplift during intra-continental orogeny primarily via differences in thermal structure. Specifically, a hotter Tian Shan lithosphere, with Moho temperature > 100 ˚C hotter than that of the proto-southern Asia, leads to an earlier and higher uplift of the Tian Shan, and much more efficient far-field stress transfer (Figs. 9b, c, 10a, 11). Faster convergence rates amplify this effect (Figs. 6, 11b). This thermal heterogeneity has been evidenced by both geophysical and geological studies. A high Moho temperature beneath the Tian Shan before its deformation at ~20–30 Myr ago is suggested based on the following observations. First, electrical conductivity of xenoliths showed that the Tian Shan was 850 ˚C at the Moho boundary before the Late Oligocene-Early Miocene initiation of deformation (Bagdassarov et al., 2011). Second, the Tian Shan is a complex terrane created by the sequential accretion of many microcontinents and island arcs in the Late Carboniferous (Burtman, 1975; Coleman, 1989; Windley et al., 1990; Carroll et al., 1990; Bagdassarov et al., 2011; Charvet et al., 2011) and has experienced continuous tectonic activities prior to India-Asia collision (Hendrix et al., 1992), which allows the presence of a warm lithosphere. Third, tomography and receiver function studies revealed a low velocity anomaly in the mantle beneath the Tian Shan, potentially representing present-day mantle upwelling (Roecker et al., 1993; Kosarev et al., 1993; Huang et al., 2006), which suggests a potentially hotter Moho for at least several million years during active upwelling. In contrast, although the proto-southern Asia also involves multiple accreted terranes that began to amalgamate northward since the Early Mesozoic (Sengor and Okurogullari, 1991; Yin and Harrison, 2000), a much lower Moho temperature of ~500–600 ˚C for the proto-southern Asia has been estimated based on the uplift rate and current elevation of the Tibetan plateau (Rey et al., 2010). From this study, the Tian Shan should have a higher Moho temperature than that of the proto-southern Asia by > 100 ˚C, which could be supported by the evidence mentioned above.

This interpretation may also be applied to the east profile, where there is apparent out-of-sequence deformation between the East Kunlun range (Oligocene-Miocene, Mock et al., 1999; Wang et al., 2004; Liu et al., 2005; Yuan et al., 2006; McRivette et al., 2019) and Qilian Shan (early Cenozoic, Yin et al., 2008; Qi et al., 2016; Zuza et al., 2016, 2019; Li et al., 2019c). Similar to the Tian Shan, the Qilian Shan consists of a series of early Paleozoic and Permian-Triassic arcs that have undergone subduction and collision, followed by Permian-Triassic closure of the Paleo-Asian Ocean to its north (Yin and Harrison, 2000; Xiao et al., 2009; Song et al., 2013; Wilde, 2015; Zuza and Yin, 2017; Wu et al., 2016, 2017; Zuza et al., 2018). This evolution history would produce a warm weak lithosphere, comparable to the situation of the Tian Shan, allowing a quick response on the stress by the far-field transfer.

Modeling results also show that a higher convergence rate amplifies the time difference in the diachronous rise pattern (Model c, Fig. 6c). When the convergence rate increases from 2.5 to 5 cm/yr, the time difference of uplift between the Tian Shan and the West Kunlun range lengthens from 5 Myr (Model a, Fig. 6b) to 13 Myr (Model c, Fig. 6c). This results may also be adopted to explain the situation on the East Kunlun-Qilian Shan profile, where geological observations show that uplift of the Qilian Shan was earlier than that of East Kunlun range by at least 10 Myr, and possibly > 20 Myr. It is possible that this out-of-sequence uplift with a larger time difference might result from faster convergence rates (> 5 cm/yr), as indicated by the Figs. 6c and A.3. That is to say, it is likely that the diachronous uplift between the East Kunlun range and Qilian Shan was driven by the similar mechanism proposed for the West Kunlun-Tian Shan profile.

In general, our modeling demonstrates that the Cenozoic intraplate orogeny of the Asian plate is controlled by the far-field effect of the India-Asia collision, while the topographic rise pattern depends on the intrinsic property of each thrust belt, such as thermal structure. The diachronous uplift of the Himalayan-Tibetan orogen, such as the West Kunlun range versus the South Tian Shan or the East Kunlun range and the Qilian Shan, is triggered by the complex pre-collisional history, including the numerous arcs and suture zones in the Tian Shan, Qilian Shan and northern Tibet.

6.4. Limitations

With the purpose of fully checking its controlling effects, a constant convergence rate (i.e., the shortening rate) was adopted from 1 to 5 cm/yr in each model. This is different from the situation that the convergence rate changes over time (Guillot et al., 2003). We also performed additional models (Figs. A.3, A.4, A.5) to investigate the effects under higher (6.5 cm/yr, the maximum, Guillot et al., 2003) or changing convergence rates. The results did not change the trend of intraplate orogeny pattern. We prefer adopting constant convergence rates in the modeling because it highlights the effects of convergence rate on the pattern of intraplate orogeny. In addition, our results suggest that the larger time lag of the diachronous rise in the East Kunlun-Qilian Shan profile than that in the West Kunlun-South Tian Shan profile (Fig. 1) could be caused by a higher convergence rate. This is consistent with the significant along-strike variation in the convergence rate in the Himalayan-Tibetan orogen (Molnar and Stock, 2009), which may be related to the rotational underthrusting of the Indian plate (Klootwijk et al., 1985).

In this study, the 2D numerical modeling was focused on representing the far-field effect and associated topographic expression of India-Asia collision in the north-south direction. The current models excluded any potential lateral extrusion or strike-slip faulting as proposed by Tapponnier et al. (1982) and numerically modeled in the previous studies (e.g., Li et al., 2013; Chen et al., 2017). In addition, to concentrate on evaluating the far-field effects, we simplified the models by integrating all accreted terranes into one homogeneous block. Both limitations do not allow us to reproduce more detailed deformation features. It is noteworthy that the setup of the lithosphere of the Tethys Ocean was only to facilitate the subsequent subduction of the Indian plate, and thus a narrow Tethys Ocean was adopted to initiate the subduction process. The simplified model configuration has successfully revealed the first-order factors leading to the diachronous uplift of the South Tian Shan and the West Kunlun range as well as the Qilian Shan and the East Kunlun range, respectively.

7. Conclusions

Two-dimensional thermo-mechanical simulations illustrate that the diachronous uplift of the Tian Shan and the West Kunlun range could be induced by the far-field effect of the India-Asia collision. A hotter Moho under the Tian Shan than that of the West Kunlun range causes the Tian Shan to deform earlier despite its distance from the collisional front, while the colder West Kunlun range resists deformation at a certain degree. When the difference in the Moho temperature exceeds 100 ˚C, the block with a hotter Moho temperature and thus a weaker lithosphere responds quicker to the convergence of the India-Asia plates. Additionally, this situation is amplified by increasing convergence rates, which promotes transmitting of the stress more efficiently through the rigid Tarim block. The modeling implies that the effects of

far-field stress transfer may first manifest in the parts of the ranges with the hottest and weakest lithosphere. The unique diachronous uplift of the Tibetan plateau and thrust belts in Asian continent's interior is controlled by the pre-collisional geology.

Author contribution

Shuang Bian: Methodology, Formal analysis, Investigation, Writing-Original Draft, Visualization; Junfeng Gong: Conceptualization, Writing-Review & Editing, Supervision, Project administration, Funding acquisition; Lin Chen: Conceptualization, Writing-Review & Editing, Supervision, Project administration, Funding acquisition; Andrew V. Zuza: Writing-Review & Editing, Funding acquisition; Hanlin Chen: Writing-Review & Editing, Funding acquisition; Xiubin Lin: Writing-Review & Editing, Funding acquisition; Xiaogan Cheng: Writing-Review & Editing, Funding acquisition; Rong Yang: Writing-Review & Editing, Funding acquisition.

Declaration of competing interest

The authors declare that they have no known competing financial interests or personal relationships that could have appeared to influence the work reported in this paper.

Acknowledgements

We are indebted to Prof. Taras Gerya for providing the code I2VIS. This study was supported by the Strategic Priority Research Program (B) of the Chinese Academy of Sciences (XDB18000000), National Natural Science Foundation of China (Grant Nos. 41472182, 41474084, 41472181, 41602210, 41330207 and 41720104003), the National Major Science and Technology Projects of China (Grant Nos. 2017ZX05008-001, 2017ZX05003-001), and National Science Foundation (EAR 1914501). The work was carried out on TianHe-1A system at National Supercomputer Center in Tianjin, China. Extensive comments and suggestions by Dr. Weronika Gorczyk, an anonymous reviewer, and Editor Dr. Zheng-Xiang Li greatly improved the manuscript.

Appendix A. Supplementary data

Supplementary data to this article can be found online at https://doi.org/10.1016/j.tecto.2019.228310.

References

Armijo, R., Tapponnier, P., Mercier, J.L., Han, T.L., 1986. Quaternary extension in southern Tibet: field observations and tectonic implications. J. Geophys. Res. 91, 13803–13872. https://doi.org/10.1029/JB091iB14p13803.

Armijo, R., Tapponnier, P., Tonglin, H., 1989. Late Cenozoic right-lateral strike-slip faulting in southern Tibet. J. Geophys. Res. 94, 2787–2838. https://doi.org/10.1029/JB094iB03p02787.

Avouac, J.P., Tapponnier, P., Bai, M., You, H., Wang, G., 1993. Active thrusting and folding along the northern Tien Shan and Late Cenozoic rotation of the Tarim relative to Dzungaria and Kazakhstan. J. Geophys. Res. 98 (B4), 6755–6804. https://doi.org/10.1029/92JB01963.

Bagdassarov, N., Batalev, V., Egorova, V., 2011. State of lithosphere beneath Tien Shan from petrology and electrical conductivity of xenoliths. J. Geophys. Res. 116, B01202. https://doi.org/10.1029/2009JB007125.

Beaumont, C., Jamieson, R.A., Nguyen, M.H., Medvedev, S., 2004. Crustal channel flows: 1. Numerical models with applications to the tectonics of the Himalayan-Tibetan orogen. J. Geophys. Res. 109 (B6), B06406. https://doi.org/10.1029/2003jb002809.

Bittner, D., Schmeling, H., 1995. Numerical modeling of melting processes and induced diapirism in the lower crust. Geophys. J. Int. 123, 59–70. https://doi.org/10.1111/j.1365-246X.1995.tb06661.x.

Bovet, P.M., Ritts, B.D., Gehrels, G., Abbink, A.O., Darby, B., Hourigan, J., 2009. Evidence of Miocene crustal shortening in the north Qilian Shan from Cenozoic stratigraphy of the western Hexi corridor, Gansu province, China. Am. J. Sci. 309 (4), 290–329. https://doi.org/10.2475/00.4009.02.

Bullen, M.E., Burbank, D.W., Garver, J.I., Abdrakhmatov, K.Y., 2001. Late Cenozoic tectonic evolution of the northwestern Tien Shan: new age estimates for the initiation of mountain building. Geol. Soc. Amer. Bull. 113 (12), 1544–1559. https://doi.org/10.1130/0016-7606(2001)113<1544:LCTEOT>2.0.CO;2.

Bullen, M.E., Burbank, D.W., Garver, J.I., 2003. Building the northern Tien Shan: integrated thermal, structural, and topographic constraints. J. Geol. 111 (2), 149–165. https://doi.org/10.1086/345840.

Burg, J.P., Gerya, T.V., 2005. The role of viscous heating in Barrovian metamorphism of collisional orogens: thermomechanical models and application to the Lepontine Dome in the Central Alps. J. Metamorph. Geol. 23, 75–95. https://doi.org/10.1111/j.1525-1314.2005.00563.x.

Burg, J.P., Davy, P., Martinod, J., 1994. Shortening of analogue models of the continental lithosphere: new hypothesis for the formation of the Tibetan plateau. Tectonics 13 (2), 475–483. https://doi.org/10.1029/93tc02738.

Burov, E.B., Watts, A.B., 2006. The long-term strength of continental lithosphere: "Jelly Sandwich" or "Crème Brûlée"? Geol. Soc. Am. Today 16 (16), 4–10.

Burtman, V.S., 1975. Structural geology of Variscan Tien Shan. Am. J. Sci. 275, 157–186.

Carroll, A.R., Liang, Y., Graham, S.A., Xiao, X., Hendrix, M.S., Chu, J.C., McKnight, C.L., 1990. Junggar Basin, northwest China: trapped late Paleozoic ocean. Tectonophysics 181, 1–14. https://doi.org/10.1016/0040-1951(90)90004-r.

Charreau, J., Chen, Y., Gilder, S., Dominguez, S., Avouac, J.P., Sen, S., Sun, D.J., Li, Y.A., Wang M., W., 2005. Magnetostratigraphy and rock magnetism of the neogene kuitun he section (northwest china): implications for late Cenozoic uplift of the Tianshan mountains. Earth Planet. Sci. Lett. 230 (1–2), 177–192. https://doi.org/10.1016/j.epsl.2004.11.002.

Charreau, J., Gilder, S., Chen, Y., Dominguez, S., Avouac, J.P., Sen, S., Jolivet, M., Li, Y.A., Wang, W.M., 2006. Magnetostratigraphy of the Yaha section, Tarim basin (China): 11 Ma acceleration in erosion and uplift of the Tian Shan mountains. Geology 34 (3), 181–184. https://doi.org/10.1130/G22106.1.

Charreau, J., Chen, Y., Gilder, S., Barrier, L., Dominguez, S., Augier, R., Sen, S., Avouac, J.P., Gallaud, A., Graveleau, F., Wang, Q.C., 2009. Neogene uplift of the Tian Shan Mountains observed in the magnetic record of the Jingou River section (northwest China). Tectonics 28 (2), 224–243. https://doi.org/10.1029/2007TC002137.

Charvet, J., Shu, L.S., Laurent-Charvet, S., Wang, B., Michel, F., Dominique, C., Chen, Y., Jong, K.D., 2011. Paleozoic tectonic evolution of the Tianshan belt, NW China. Sci. China Ser. D Earth Sci. 54 (2), 166–184. https://doi.org/10.1007/s11430-010-4138-1.

Chen, L., Gerya, T.V., 2016. The role of lateral lithospheric strength heterogeneities in orogenic plateau growth: Insights from 3-D thermo-mechanical modeling. J. Geophys. Res. 121 (4), 3118–3138. https://doi.org/10.1002/2016jb012872.

Chen, L., Capitanio, F.A., Liu, L., Gerya, T.V., 2017. Crustal rheology controls on the Tibetan plateau formation during India-Asia convergence. Nat. Commun. 8, 15992. https://doi.org/10.1038/ncomms15992.

Cheng, F., Jolivet, M., Fu, S.T., Zhang, C.H., Zhang, Q.Q., Guo, Z.J., 2016. Large-scale displacement along the Altyn Tagh Fault (North Tibet) since its Eeocene initiation: insight from detrital zircon U-Pb geochronology and subsurface data. Tectonophysics 677–678, 261–279. https://doi.org/10.1016/j.tecto.2016.04.023.

Cheng, F., Garzione, C., Jolivet, M., Guo, Z.J., Zhang, D.W., Zhang, C.H., 2018. A new sediment accumulation model of Cenozoic depositional ages from the Qaidam basin, Tibetan Plateau. J. Geophys. Res. 123 (11), 3101–3121. https://doi.org/10.1029/2018jf004645.

Clark, M.K., Farley, K.A., Zheng, D.W., Wang, Z.C., Duvall, A.R., 2010. Early Cenozoic faulting of the northern Tibetan Plateau margin from apatite (U-Th)/He ages. Earth Planet. Sci. Lett. 296 (1–2), 78–88. https://doi.org/10.1016/j.epsl.2010.04.051.

Clauser, C., Huenges, E., 1995. Thermal conductivity of rocks and minerals. In: Ahrens, T.J. (Ed.), Rock Physics and Phase Relations. American Geophysical Union, Washington, pp. 105–126.

Coleman, R.G., 1989. Continental growth of northwest China. Tectonics 8 (3), 621–635. https://doi.org/10.1029/TC008i003p00621.

Cowgill, E.S., 2001. Tectonic Evolution of the Altyn Tagh-western Kunlun Fault System, Northwestern China. Doctoral dissertation. University of California, Los Angeles.

Crameri, F., Schmeling, H., Golabek, G.J., Duretz, T., Orendt, R., Buiter, S.J.H., May, D.A., Kaus, B.J.P., Gerya, T.V., Tackley, P.L., 2012. A comparison of numerical surface topography calculations in geodynamic modelling: an evaluation of the 'sticky air' method. Geophys. J. Int. 189 (1), 38–54. https://doi.org/10.1111/j.1365-246x.2012.05388.x.

Dai, J.G., Wang, C.S., Hourigan, J., Santosh, M., 2013. Multi-stage tectono-magmatic events of the eastern Kunlun range, northern Tibet: insights from U-Pb geochronology and (U-Th)/He thermochronology. Tectonophysics 599, 97–106. https://doi.org/10.1016/j.tecto.2013.04.005.

Dayem, K.E., Molnar, P., Clark, M.K., Houseman, G.A., 2009. Far-field lithospheric deformation in Tibet during continental collision. Tectonics 28 (6), TC6005. https://doi.org/10.1029/2008tc002344.

De Grave, J., Buslov, M.M., Haute, P.V.D., 2007. Distant effects of India-Eurasia convergence and Mesozoic intracontinental deformation in central Asia: constraints from apatite fission-track thermochronology. J. Asian Earth Sci. 29 (2–3), 188–204. https://doi.org/10.1016/j.jseaes.2006.03.001.

De Grave, J., Glorie, S., Buslov, M.M., Izmer, A., Fournier-Carrie, A., Batalev, V.Y., Vanhaecke, F., Elburg, M., Van den haute, P., 2011. The thermo-tectonic history of the Song-Kul plateau, Kyrgyz Tien Shan: constraints by apatite and titanite thermochronometry and zircon U/Pb dating. Gondwana Res. 20 (4), 745–763. https://doi.org/10.1016/j.gr.2011.03.011.

Dewey, J.F., Burke, K.C.A., 1973. Tibetan, Variscan, and Precambrian basement reactivation: products of continental collision. J. Geol. 81 (6), 683–692. https://doi.org/10.1086/627920.

Duvall, A.R., Clark, M.K., Kirby, E., Farley, K.A., Craddock, W.H., Li, C.Y., Yuan, D.Y., 2013. Low-temperature thermochronometry along the Kunlun and Haiyuan faults, NE Tibetan plateau: evidence for kinematic change during late-stage orogenesis.

Tectonics 32 (5), 1190–1211. https://doi.org/10.1002/tect.20072.
England, P., Houseman, G., 1985. Role of lithospheric strength heterogeneities in the tectonics of Tibet and neighbouring regions. Nature 315 (6017), 297–301. https://doi.org/10.1038/315297a0.
England, P., Houseman, G., 1986. Finite strain calculations of continental deformation: 2. Comparison with the India-Asia collision zone. J. Geophys. Res. 91 (B3), 3664–3676. https://doi.org/10.1029/JB091iB03p03664.
England, P., McKenzie, D., 1982. A thin viscous sheet model for continental deformation. Geophys. J. R. Astron. Soc. 70, 295–321. https://doi.org/10.1111/j.1365-246X.1982.tb04969.x.
Gao, R., Hou, H.S., Cai, X.Y., Knapp, H.J., He, R.Z., Liu, J.K., Xiong, X.S., Guan, Y., Li, W.H., Zeng, L.S., Roecker, S.W., 2013. Fine crustal structure beneath the junction of the southwest Tian Shan and Tarim basin, NW china. Lithosphere 5 (4), 382–392. https://doi.org/10.1130/l248.1.
Gerya, T.V., Perchuk, L.L., Burg, J.P., 2008. Transient hot channels: perpetrating and regurgitating ultrahigh-pressure, high-temperature crust-mantle associations in collision belts. Lithos 103, 236–256. https://doi.org/10.1016/j.lithos.2007.09.017.
Glorie, S., Grave, J.D., Buslov, M.M., Elburg, M.A., Stockli, D.F., Gerdes, A., Van dem haute, P., 2010. Multi-method chronometric constraints on the evolution of the Northern Kyrgyz Tien Shan granitoids (central Asian orogenic belt): from emplacement to exhumation. J. Asian Earth Sci. 38 (3–4), 131–146. https://doi.org/10.1016/j.jseaes.2009.12.009.
Gerya, T.V., Yuen, D.A., 2003a. Characteristics-based marker-in-cell method with conservative finite-differences schemes for modeling geological flows with strongly variable transport properties. Phys. Earth Planet. Inter. 140, 295–320. https://doi.org/10.1016/j.pepi.2003.09.006.
Gerya, T.V., Yuen, D.A., 2003b. Rayleigh-Taylor instabilities from hydration and melting propel 'cold plumes' at subduction zones. Earth Planet. Sci. Lett. 212, 47–62. https://doi.org/10.1016/S0012-821X(03)00265-6.
Glorie, S., De Grave, J., Buslov, M.M., Zhimulev, F.I., Stockli, D.F., Batalev, V.Y., Lzmer, A., Van dem haute, P., Vanhaecke, F., Elburg, M.A., 2011. Tectonic history of the Kyrgyz South Tien Shan (Atbashi-Inylchek) suture zone: the role of inherited structures during deformation-propagation. Tectonics 30 (6), TC6016. https://doi.org/10.1029/2011TC002949.
Gueydan, F., Morency, C., Brun, J.P., 2008. Continental rifting as a function of lithosphere mantle strength. Tectonophysics 460, 83–93. https://doi.org/10.1016/j.tecto.2008.08.012.
Guillot, S., Garzanti, E., Baratoux, D., Marquer, D., Mahéo, G., Sigoyer, J.D., 2003. Reconstructing the total shortening history of the NW Himalaya. Geochem. Geophys. Geosyst. 4 (7), 1–22. https://doi.org/10.1029/2002gc000484.
Guo, Z.J., Jiemin, L.U., Zhang, Z.C., 2009. Cenozoic exhumation and thrusting in the northern Qilian Shan, northeastern margin of the Tibetan plateau: constraints from sedimentological and apatite fission-track data. Acta Geol. Sin. Engl. 83 (3), 562–579. https://doi.org/10.1111/j.1755-6724.2009.00045.x.
Heermance, R.V., Chen, J., Burbank, D.W., Wang, C.S., 2007. Chronology and tectonic controls of late tertiary deposition in the southwestern Tian Shan foreland, NW China. Basin Res. 19 (4), 599–632. https://doi.org/10.1111/j.1365-2117.2007.00339.x.
Hendrix, M.S., Graham, S.A., Carroll, A.R., Sobel, E.R., Mcknight, C.L., Schulein, B.J., Wang, Z.X., 1992. Sedimentary record and climatic implications of recurrent deformation in the Tian Shan: evidence from Mesozoic strata of the north Tarim, south Junggar, and Turpan basins, northwest China. Geol. Soc. Am. Bull. 104 (1), 53–79. https://doi.org/10.1130/0016-7606(1992)104<0053:sracio>2.3.co;2.
Hendrix, M.S., Dumitru, T.A., Graham, S.A., 1994. Late Oligocene-early Miocene unroofing in the Chinese Tian Shan: an early effect of the India-Asia collision. Geology 22 (6), 487–490. https://doi.org/10.1130/0091-7613(1994)022<0487:LOEMUI>2.3.CO;2.
Hess, P.C., 1989. Origin of Igneous Rocks. Harvard University Press, London.
Hirschmann, M.M., 2000. Mantle solidus: experimental constraints and the effects of peridotite composition. Geochem. Geophys. Geosyst. 1 (10). https://doi.org/10.1029/2000GC000070.
Hodges, K.V., Wobus, C., Ruhl, K., Schildgen, T., Whipple, K., 2004. Quaternary deformation, river steepening, and heavy precipitation at the front of the higher Himalayan ranges. Earth Planet. Sci. Lett. 220 (3), 379–389. https://doi.org/10.1016/s0012-821x(04)00063-9.
Hofmeister, A.M., 1999. Mantle values of thermal conductivity and the geotherm from phonon lifetimes. Science 283, 1699–1706. https://doi.org/10.1126/science.283.5408.1699.
Huang, B.C., Piper, J.D.A., Peng, S.T., Liu, T., Li, Z., Wang, Q.C., Zhu, R.X., 2006. Magnetostratigraphic study of the Kuche depression, Tarim Basin, and Cenozoic uplift of the Tian Shan Range, Western China. Earth Planet. Sci. Lett. 251 (3–4), 346–364. https://doi.org/10.1016/j.epsl.2006.09.020.
Huangfu, P.P., Li, Z.H., Gerya, T., Fan, W.M., Zhang, K.J., Zhang, H., Shi L., Y., 2018. Multi-terrane structure controls the contrasting lithospheric evolution beneath the western and central-eastern Tibetan plateau. Nat. Commun. 9 (1), 1–11. https://doi.org/10.1038/s41467-018-06233-x.
Jepson, G., Glorie, S., Konopelko, D., Gillespie, J., Daniš́k, M., Evans, N.J., Mamadjanov, Y., Collins, A.S., 2017. Thermochronological insights into the structural contact between the Tian Shan and Pamirs, Tajikistan. Terra Nova 30 (2), 95–104. https://doi.org/10.1111/ter.12313.
Jiang, X.D., Li, Z.X., 2014. Seismic reflection data support episodic and simultaneous growth of the Tibetan Plateau since 25 Myr. Nat. Commun. 5, 5453. https://doi.org/10.1038/ncomms6453.
Johannes, W., 1985. The significance of experimental studies for the formation of migmatites. In: Ashworth, J.R. (Ed.), Migmatites. Blackie, Glasgow, pp. 36–85.
Jolivet, M., Brunel, M., Seward, D., Xu, Z., Yang, J., Roger, F., Tapponnier, P., Malavieille, J., Arnaud, N., Wu, C., 2001. Mesozoic and Cenozoic tectonics of the northern edge of the Tibetan Plateau: fission-track constraints. Tectonophysics 343 (1), 111–134. https://doi.org/10.1016/S0040-1951(01)00196-2.
Kao, H., Gao, R., Rau, R.J., Shi, D.N., Chen, R.Y., Guan, Y., Wu, F.T., 2001. Seismic image of the Tarim basin and its collision with Tibet. Geology 29 (7), 575–578. https://doi.org/10.1130/0091-7613(2001)029<0575:siottb>2.0.co;2.
Kapp, P., Yin, A., Harrison, T.M., Ding, L., 2005. Cretaceous-Tertiary shortening, basin development, and volcanism in central Tibet. Geol. Soc. Am. Bull. 117 (7), 865–878. https://doi.org/10.1130/B25595.1.
Kelly, S., Butler, J.P., Beaumont, C., 2016. Continental collision with a sandwiched accreted terrane: insights into Himalayan-Tibetan lithospheric mantle tectonics? Earth Planet. Sci. Lett. 455, 176–195. https://doi.org/10.1016/j.epsl.2016.08.039.
Klootwijk, C.T., Conaghan, P.J., Powell, C.M., 1985. The Himalayan arc: large-scale continental subduction, oroclinal bending and back-arc spreading. Earth Planet. Sci. Lett. 75 (2), 167–183.
Kosarev, G.L., Petersen, N.V., Vinnik, L.P., Roecker, S.W., 1993. Receiver functions for the Tien Shan analog broadband network: contrasts in the evolution of structures across the Talasso-Fergana fault. J. Geophys. Res. 98 (B3), 4437–4448. https://doi.org/10.1029/92JB02651.
Kosarev, G., Kind, R., Sobolev, S.V., Yuan, X., Hanka, W., Oreshin, S., 1999. Seismic evidence for a detached Indian lithospheric mantle beneath Tibet. Science 283 (5406), 1306–1309. https://doi.org/10.1126/science.283.5406.1306.
Kumar, P., Yuan, X., Kind, R., Kosarev, G., 2005. The lithosphere-asthenosphere boundary in the Tien Shan-Karakoram region from S receiver functions: evidence for continental subduction. Geophys. Res. Lett. 32 (7), L07305.
Lewis, C.L.E., 1990. Thermal history of the Kunlun batholith, N. Tibet, and implications for uplift of the Tibetan plateau. Nucl. Tracks Radiat. Meas. 17 (3), 301–307. https://doi.org/10.1016/1359-0189(90)90050-8.
Li, G., Pettke, T., Chen, J., 2011. Increasing Nd isotopic ratio of Asian dust indicates progressive uplift of the north Tibetan Plateau since the middle Miocene. Geology 39 (3), 199–202. https://doi.org/10.1130/g31734.1.
Li, C., Wang, A.L., Wang, L.S., 2019b. Tectonostratigraphic history of the southern Tian Shan, western China, from seismic reflection profiling. J. Asian Earth Sci. 172, 101–114. https://doi.org/10.1016/j.jseaes.2018.08.017.
Li, Z.H., Xu, Z., Gerya, T., Burg, J.P., 2013. Collision of continental corner from 3-d numerical modeling. Earth Planet. Sci. Lett. 380, 98–111. https://doi.org/10.1016/j.epsl.2013.08.034.
Li, B., Chen, X.H., Zuza, A.V., Hu, D.G., Ding, W.C., Huang, P.H., Xu, S.L., 2019a. Cenozoic cooling history of the North Qilian Shan, northern Tibetan Plateau and the initiation of the Haiyuan fault: constraints from apatite- and zircon fission track thermochronology. Tectonophysics 751, 109–124. https://doi.org/10.1016/j.tecto.2018.12.005.
Li, Z.H., Liu, M., Gerya, T., 2016. Lithosphere delamination in continental collisional orogens: a systematic numerical study. J. Geophys. Res. 121, 5186–5211. https://doi.org/10.1002/2016JB013106.
Li, B., Zuza, A.V., Chen, X.H., Hu, D.G., Shao, Z.G., 2019c. Cenozoic multi-pulse range growth in the Qilian Shan, northern Tibet plateau, as constrained by geologic mapping and apatite fission track thermochronology. GSA Annual Meet. Abstr. 130–134.
Liu, Y.J., Genser, J., Neubauer, F., Jin, W., Ge, X., Handler, R., Takasu, A., 2005. $^{40}Ar/^{39}Ar$ mineral ages from basement rocks in the Eastern Kunlun Mountains, NW China, and their tectonic implications. Tectonophysics 398 (3–4), 199–224. https://doi.org/10.1016/j.tecto.2005.02.007.
Lu, H.J., Wang, E., Shi, X.H., Meng, K., 2012. Cenozoic tectonic evolution of the Elashan range and its surroundings, northern Tibetan Plateau as constrained by paleomagnetism and apatite fission track analyses. Tectonophysics 580, 150–161. https://doi.org/10.1016/j.tecto.2012.09.013.
McRivette, M.W., Yin, A., Chen, X.H., Gehrels, G.E., 2019. Cenozoic basin evolution of the central Tibetan plateau as constrained by U-Pb detrital zircon geochronology, sandstone petrology, and fission-track thermochronology. Tectonophysics 751, 150–179. https://doi.org/10.1016/j.tecto.2018.12.015.
Métivier, F., Gaudemer, Y., 1997. Mass transfer between eastern Tien Shan and adjacent basins (central Asia): constraints on regional tectonics and topography. Geophys. J. Int. 128 (1), 1–17.
Mock, C., Arnaud, N.O., Cantagrel, J.M., 1999. An early unroofing in northeastern Tibet? Constraints from $^{40}Ar/^{39}Ar$ thermochronology on granitoids from the eastern Kunlun range (Qianghai, NW China). Earth Planet. Sci. Lett. 171 (1), 107–122. https://doi.org/10.1016/s0012-821x(99)00133-8.
Molnar, P., Stock, J.M., 2009. Slowing of India's convergence with Eurasia since 20 Ma and its implications for Tibetan mantle dynamics. Tectonics 28 (3), TC3001. https://doi.org/10.1029/2008TC002271.
Molnar, P., Tapponnier, P., 1975. Cenozoic tectonics of Asia: effects of a continental collision. Science 189 (4201), 419–426. https://doi.org/10.1126/science.189.4201.419.
Molnar, P., Tapponnier, P., 1978. Active tectonics of Tibet. J. Geophys. Res. 83 (B11), 5361–5375. https://doi.org/10.1029/JB083iB11p05361.
Murphy, M.A., Yin, A., Harrison, T.M., Dürr, S.B., Chen, Z., Ryerson, F.J., Kidd, W.S.F., Wang, X., Zhou, X., 1997. Did the Indo-Asian collision alone create the Tibetan plateau? Geology 25 (8), 719–722. https://doi.org/10.1130/0091-7613(1997)025<0719:DTIACA>2.3.CO;2.
Neil, E.A., Houseman, G.A., 1997. Geodynamics of the Tarim Basin and the Tian Shan in central Asia. Tectonics 16 (4), 571–584. https://doi.org/10.1029/97tc01413.
Nelson, K.D., Zhao, W.J., Brown, L.D., Kuo, J., Che, J.K., Liu, X.W., Klemperer, S.L., Makovsky, Y., Meissner, R., Mechie, J., Kind, R., Wenzel, F., Hi, J., Nabelek, J., Chen, L.S., Tan, H.D., Wei, W.B., Jones, A.G., Booker, J., Unsworth, M., Kidd, W.S.F., Hauck, M., Alsdorf, D., Ross, A., Cogan, M., Wu, C.D., Sandvol, E., Edwards, M., 1996. Partially molten middle crust beneath southern Tibet: synthesis of project INDEPTH

results. Science 274, 1684–1688. https://doi.org/10.1126/science.274.5293.1684.
Poli, S., Schmidt, M.W., 2002. Petrology of subducted slabs. Annu. Rev. Earth Planet. Sci. 30, 207–237. https://doi.org/10.1146/annurev.earth.30.091201.140550.
Pusok, A.E., Kaus, B.J.P., 2015. Development of topography in 3-D continental-collision models. Geochem. Geophys. Geosyst. 16 (5), 1378–1400. https://doi.org/10.1002/2015GC005732.
Qi, B.S., Hu, D.G., Yang, X.X., Zhang, Y.L., Tan, C.X., Zhang, P., Feng, C.J., 2016. Apatite fission track evidence for the Cretaceous-Cenozoic cooling history of the Qilian Shan (NW China) and for stepwise northeastward growth of the northeastern Tibetan Plateau since early Eocene. J. Asian Earth Sci. 124, 28–41. https://doi.org/10.1016/j.jseaes.2016.04.009.
Ranalli, G., 1995. Rheology of the Earth: Deformation and Flow Processes in Geophysics and Geodynamics, 2nd ed. Chapman and Hall, London, UK.
Rey, P.F., Teyssier, C., Whitney, D.L., 2010. Limit of channel flow in orogenic plateaux. Lithosphere 2 (5), 328–332. https://doi.org/10.1130/L114.1.
Ritts, B.D., Yue, Y., Graham, S.A., Sobel, E.R., Abbink, O.A., Stockli, D., 2008. From sea level to high elevation in 15 million years: uplift history of the northern Tibetan plateau margin in the Altun Shan. Am. J. Sci. 308 (5), 657–678. https://doi.org/10.2475/05.2008.01.
Roecker, S.W., Sabitova, T.M., Vinnik, L.P., Burmakov, Y.A., Golvanov, M.I., Mamatkanova, R., Munirova, L., 1993. Three-dimensional elastic wave velocity structure of the western and central Tien Shan. J. Geophys. Res. 98 (B9), 15779–15795. https://doi.org/10.1029/93JB01560.
Royden, L., 1996. Coupling and decoupling of crust and mantle in convergent orogens: implications for strain partitioning in the crust. J. Geophys. Res. 101 (B8), 17679–17705. https://doi.org/10.1029/96JB00951.
Schmalholz, S.M., Kaus, B.J.P., Burg, J.P., 2009. Stress-strength relationship in the lithosphere during continental collision. Geology 37 (9), 775–778. https://doi.org/10.1130/G25678A.1.
Schmeling, H., Babeyko, A.Y., Enns, A., Faccenna, C., Funiciello, F., Gerya, T., Golabek, G.J., Grigull, S., Kaus, B.J.P., Morra, G., Schmalholz, S.M., van Hunen, J., 2008. A benchmark comparison of spontaneous subduction models: towards a free surface. Phys. Earth Planet. Inter. 171, 198–223. https://doi.org/10.1016/j.pepi.2008.06.028.
Schmidt, M.W., Poli, S., 1998. Experimentally based water budgets for dehydrating slabs and consequences for arc magma generation. Earth Planet. Sci. Lett. 163 (1–4), 361–379.
Sengor, A.M.C., Okurogullari, A.H., 1991. The role of accretionary wedge in the growth of continents: Asiatic examples from Argand to plate tectonics. Ecol. Geol. Helv. 84, 535–597.
Shi, W.B., Wang, F., Yang, L.Y., Wu, L., Zhang, W.B., 2018. Diachronous growth of the Altyn Tagh Mountains: constraints on propagation of the Northern Tibetan margin from (U-Th)/He dating. J. Geophys. Res. 123, 6000–6018. https://doi.org/10.1029/2017JB014844.
Sobel, E.R., Dumitru, T.A., 1997. Thrusting and exhumation around the margins of the western Tarim basin during the India-Asia collision. J. Geophys. Res. 102 (B3), 5043–5063. https://doi.org/10.1029/96jb03267.
Sobel, E.R., Chen, J., Heermance, R.V., 2006. Late Oligocene-Early Miocene initiation of shortening in the Southwestern Chinese Tian Shan: implications for Neogene shortening rate variations. Earth Planet. Sci. Lett. 247 (1-2), 70–81. https://doi.org/10.1016/j.epsl.2006.03.048.
Sobel, E.R., Chen, J., Schoenbohm, L.M., Thiede, R., Stockli, D.F., Sudo, M., Strecker, M.R., 2013. Oceanic-style subduction controls late Cenozoic deformation of the Northern Pamir orogen. Earth Planet. Sci. Lett. 363 (2), 204–218. https://doi.org/10.1016/j.epsl.2012.12.009.
Song, S.G., Niu, Y., Su, L., Xia, X., 2013. Tectonics of the North Qilian orogen, NW China. Gondwana Res. 23 (4), 1378–1401. https://doi.org/10.1016/j.gr.2012.02.004.
Sun, J.M., Zhu, R.X., An, Z.S., 2005. Tectonic uplift in the northern Tibetan plateau since 13.7 Ma ago inferred from molasse deposits along the Altyn Tagh Fault. Earth Planet. Sci. Lett. 235 (3–4), 641–653. https://doi.org/10.1016/j.epsl.2005.04.034.
Tada, R., Zheng, H.B., Sugiura, N., Isozaki, Y., Hasegawa, H., Sun, Y.B., Yang, W.G., Wang, K., Toyoda, S., 2010. Desertification and dust emission history of the Tarim basin and its relation to the uplift of northern Tibet. Geol. Soc. London Spec. Publ. 342 (1), 45–65. https://doi.org/10.1144/SP342.5.
Tang, Z.H., Ding, Z.L., White, P.D., Dong, X.X., Ji, J.L., Jiang, H.C., Luo, P., Wang, X., 2011. Late Cenozoic central Asian drying inferred from a palynological record from the northern Tian Shan. Earth Planet. Sci. Lett. 302 (3), 439–447. https://doi.org/10.1016/j.epsl.2010.12.042.
Tapponnier, P., Peltzer, G., Dain, A.Y.L., Armijo, R., Cobbold, P., 1982. Propagating extrusion tectonics in Asia: new insights from simple experiments with plasticine. Geology 10 (10), 611–616. https://doi.org/10.1130/0091-7613(1982)10<611:petian>2.0.co;2.
Tapponnier, P., Xu, Z.Q., Roger, F., Meyer, B., Arnaud, N., Wittlinger, G., Yang, J.S., 2001. Oblique stepwise rise and growth of the Tibet plateau. Science 294 (5547), 1671–1677. https://doi.org/10.1126/science.105978.
Tunini, L., Jiménez-Munt, I., Fernandez, M., Vergés, J., Villaseñor, A., Melchiorre, M., Afonso, J.C., 2016. Geophysical-petrological model of the crust and upper mantle in the India-Eurasia collision zone. Tectonics 35 (7), 1642–1669. https://doi.org/10.1002/2016TC004161.
Turcotte, D.L., Schubert, G., 2002. Geodynamics. Cambridge University Press, Cambridge.
Vassallo, R., Jolivet, M., Ritz, J.F., Braucher, R., Larroque, C., Sue, C., Todbileg, M., Javkhlanbold, D., 2007. Uplift age and rates of the Gurvan Bogd system (Gobi-Altay) by apatite fission track analysis. Earth Planet. Sci. Lett. 259 (3–4), 333–346. https://doi.org/10.1016/j.epsl.2007.04.047.
Vilotte, J.P., Daignieres, M., Madariaga, R., Zienkiewicz, O.C., 1984. The role of a heterogeneous inclusion during continental collision. Phys. Earth Planet. Inter. 36 (3–4), 236–259.
Wang, F., Lo, C.H., Li, Q., Yeh, M.W., Wan, J.L., Zheng, D.W., Wang, E., 2004. Onset timing of significant unroofing around Qaidam basin, northern Tibet, China: constraints from $^{40}Ar/^{39}Ar$ and FT thermochronology on granitoids. J. Asian Earth Sci. 24 (1), 59–69. https://doi.org/10.1016/j.jseaes.2003.07.004.
Wang, X., Suppe, J., Guan, S.W., Hubert-Ferrari, A., Gonzalez-Mieres, R., Jia, C.Z., 2011. Cenozoic structure and tectonic evolution of the Kuqa fold belt, southern Tianshan, China. AAPG Mem. 215–243. https://doi.org/10.1306/13251339M94389.
Wang, F., Feng, H.L., Shi, W.B., Zhang, W.B., Wu, L., Yang, L.K., Wang, Y.Z., Zhang, Z.G., Zhu, R.X., 2016. Relief history and denudation evolution of the northern Tibet margin: constraints from $^{40}Ar/^{39}Ar$ and (U-Th)/He dating and implications for far-field effect of rising plateau. Tectonophysics 675, 196–208. https://doi.org/10.1016/j.tecto.2016.03.001.
Wang, F., Shi, W.B., Zhang, W.B., Wu, L., Yang, L.K., Wang, Y.Z., Zhu, R.X., 2017. Differential growth of the northern Tibetan margin: evidence for oblique stepwise rise of the Tibetan plateau. Sci. Rep. 7, 41164. https://doi.org/10.1038/srep41164.
Wang, E., Wan, J.L., Liu, J.Q., 2003b. Late Cenozoic geological evolution of the foreland basin bordering the West Kunlun range in Pulu area: constraints on timing of uplift of northern margin of the Tibetan Plateau. J. Geophys. Res. 108 (B8), 2401. https://doi.org/10.1029/2002jb001877.
Wang, X.M., Wang, B.Y., Qiu, Z.X., Xie, G.P., Xie, J.Y., Downs, W., et al., 2003a. Danghe area (western Gansu, China) biostratigraphy and implications for depositional history and tectonics of northern Tibetan Plateau. Earth Planet. Sci. Lett. 208 (3–4), 253–269. https://doi.org/10.1016/s0012-821x(03)00047-5.
Wilde, S.A., 2015. Final amalgamation of the central Asian orogenic belt in NE china: Paleo-Asian ocean closure versus Paleo-Pacific plate subduction-a review of the evidence. Tectonophysics 662, 345–362. https://doi.org/10.1016/j.tecto.2015.05.006.
Windley, B.F., Allen, M.B., Zhang, C., Zhao, Z.Y., Wang, G.R., 1990. Paleozoic accretion and Cenozoic redeformation of the Chinese Tien Shan Range, central Asia. Geology 18 (2), 128–131. https://doi.org/10.1130/0091-7613(1990)018<0128:PAACRO>2.3.CO;2.
Wu, L., Xiao, A.C., Ma, D.D., Li, H.G., Xu, B., Shen, Y., Mao, L.G., 2014. Cenozoic fault systems in southwest Qaidam Basin, northeastern Tibetan Plateau: geometry, temporal development, and significance for hydrocarbon accumulation. AAPG Bull. 98 (6), 1213–1234. https://doi.org/10.1306/11131313087.
Wu, C., Yin, A., Zuza, A.V., Zhang, J., Liu, W., Ding, L., 2016. Pre-Cenozoic geologic history of the central and northern Tibetan Plateau and the role of Wilson cycles in constructing the Tethyan orogenic system. Lithosphere 8 (3), 254–292. https://doi.org/10.1130/L494.1.
Wu, C., Zuza, A.V., Yin, A., Liu, C.F., Reith, R.C., Zhang, J.Y., Liu, W.C., Zhou, Z.G., 2017. Geochronology and geochemistry of Neoproterozoic granitoids in the central Qilian Shan of northern Tibet: reconstructing the amalgamation processes and tectonic history of Asia. Lithosphere 9 (4), 609–636. https://doi.org/10.1130/L640.1.
Wu, C., Zuza, A.V., Zhou, Z.G., Yin, A., McRivette, M.W., Chen, X.H., Ding, L., Geng, J.Z., 2019. Mesozoic-Cenozoic evolution of the Eastern Kunlun Range, central Tibet, and implications for basin evolution during the Indo-Asian collision. Lithosphere 11 (4), 524–550 (doi:0000-0003-0647-3530).
Xiao, W.J., Windley, B.F., Yong, Y., Yan, Z., Yuan, C., Liu, C.Z., Li, J.L., 2009. Early Paleozoic to Devonian multipleaccretionary model for the Qilian Shan, NW China. J. Asian Earth Sci. 35 (3–4), 323–333. https://doi.org/10.1016/j.jseaes.2008.10.001.
Yin, A., 2000. Mode of Cenozoic east-west Extension in Tibet suggests a common origin of rifts in Asia during Indo-Asian collision. J. Geophys. Res. 105, 21745–21759. https://doi.org/10.1029/2000JB900168.
Yin, A., Harrison, T.M., 2000. Geologic evolution of the Himalayan-Tibetan orogen. Annu. Rev. Earth Planet. Sci. 28 (28), 211–280. https://doi.org/10.1146/annurev.earth.28.1.211.
Yin, A., Nie, S., Craig, P., Harrison, T.M., Ryerson, F.J., Qian, X.L., Geng, Y., 1998. Late Cenozoic tectonic evolution of the southern Chinese Tian Shan. Tectonics 17 (1), 1–27. https://doi.org/10.1029/97tc03140.
Yin, A., Rumelhart, P.E., Butler, R., Cowgill, E., Harrison, T.M., Foster, D.A., Ingersoll, R.V., Zhang, Q., Zhou, X.Q., Wang, X.F., Hanson, A., Raza, A., 2002. Tectonic history of the Altyn Tagh Fault system in northern Tibet inferred from Cenozoic sedimentation. Geol. Soc. Am. Bull. 114 (10), 1257–1295. https://doi.org/10.1130/0016-7606(2002)114<1257:THOTAT>2.0.CO;2.
Yin, A., Dang, Y.Q., Zhang, M., McRivette, M.W., Burgess, W.P., Chen, X.H., 2007. Cenozoic tectonic evolution of qaidam basin and its surrounding regions (part 2): wedge tectonics in southern Qaidam basin and the Eastern Kunlun range. Geol. Soc. Am. Spec. 433, 369–390. https://doi.org/10.1130/2007.2433(18).
Yin, A., Dang, Y.Q., Zhang, M., Chen, X.H., McRivette, M.W., 2008. Cenozoic tectonic evolution of the Qaidam basin and its surrounding regions (part 3): structural geology, sedimentation, and regional tectonic reconstruction. Geol. Soc. Am. Bull. 120 (7–8), 847–876. https://doi.org/10.1130/B26232.1.
Yuan, W.M., Zhang, X.T., Dong, J.Q., Tang, Y.H., Yu, F.S., Wang, S.C., 2003. A new vision of the intracontinental evolution of the eastern Kunlun Mountains, Northern Qinghai-Tibet plateau, China. Radiat. Meas. 36 (1–6), 357–362. https://doi.org/10.1016/s1350-4487(03)00151-3.
Yuan, W., Dong, J., Shicheng, W., Carter, A., 2006. Apatite fission track evidence for Neogene uplift in the eastern Kunlun Mountains, northern Qinghai-Tibet Plateau, China. J. Asian Earth Sci. 27 (6), 847–856. https://doi.org/10.1016/j.jseaes.2005.09.002.
Zhang, Z., Yang, L., Teng, J., Badal, J., 2011. An overview of the earth crust under China. Earth Sci. Rev. 104 (1), 143–166. https://doi.org/10.1016/j.earscirev.2010.10.003.
Zhang, T., Fang, X.M., Song, C.H., Appel, E., Wang, Y.D., 2014. Cenozoic tectonic deformation and uplift of the south Tian Shan: implications from magnetostratigraphy and balanced cross-section restoration of the Kuqa depression. Tectonophysics 628,

172–187. https://doi.org/10.1016/j.tecto.2014.04.044.
Zhang, J., Wang, Y.N., Zhang, B.H., Zhao, H., 2015. Evolution of the NE Qinghai-Tibetan Plateau, constrained by the apatite fission track ages of the mountain ranges around the Xining Basin in NW China. J. Asian Earth Sci. 97, 10–23. https://doi.org/10.1016/j.jseaes.2014.10.002.
Zheng, H.B., Powell, C.M., An, Z.S., Zhou, J., Dong, G.R., 2000. Pliocene uplift of the northern Tibetan Plateau. Geology 28 (8), 715–718.
Zheng, H.B., Huang, X.T., Butcher, K., 2006. Lithostratigraphy, petrography and facies analysis of the Late Cenozoic sediments in the foreland basin of the west Kunlun. Palaeogeogr. Palaeoclimatol. Palaeoecol. 241 (1), 61–78. https://doi.org/10.1016/j.palaeo.2006.06.015.
Zheng, D.W., Clark, M.K., Zhang, P.Z., Zheng, W.J., Farley, K.A., 2010. Erosion, fault initiation and topographic growth of the north Qilian Shan (northern Tibetan plateau). Geosphere 6 (6), 937–941. https://doi.org/10.1130/GES00523.1.
Zheng, D.W., Wang, W.T., Wan, J.L., Yuan, D.Y., Liu, C.R., Zheng, W.J., 2017. Progressive northward growth of the northern Qilian Shan-Hexi Corridor (northeastern Tibet) during the Cenozoic. Lithosphere 9 (3), L587.1. https://doi.org/10.1130/L587.1.
Zhu, D.C., Zhao, Z.D., Niu, Y.L., Dilek, Y., Hou, Z.Q., Mo, X.X., 2013. The origin and pre-Cenozoic evolution of the Tibetan Plateau. Gondwana Res. 23 (4), 1429–1454. https://doi.org/10.1016/j.gr.2012.02.002.
Zhuang, G., Hourigan, J.K., Ritts, B.D., Kent-Corson, M.L., 2011. Cenozoic multiple-phase tectonic evolution of the northern Tibetan Plateau: Constraints from sedimentary records from Qaidam basin, Hexi Corridor, and Subei basin, northwest China. Am. J. Sci. 311 (2), 116–152. https://doi.org/10.2475/02.2011.02.
Zhuang, G.S., Johnstone, S.A., Hourigan, J., Ritts, B., Robinson, A., Sobel, E.R., 2018. Understanding the geologic evolution of Northern Tibetan Plateau with multiple thermochronometers. Gondwana Res. 58, 195–210. https://doi.org/10.1016/j.gr.2018.02.014.
Zuza, A.V., Yin, A., 2016. Continental deformation accommodated by non-rigid passive bookshelf faulting: an example from the Cenozoic tectonic development of northern Tibet. Tectonophysics 677, 227–240. https://doi.org/10.1016/j.tecto.2016.04.007.
Zuza, A.V., Yin, A., 2017. Balkatach hypothesis: a new model for the evolution of the Pacific, Tethyan, and Paleo-Asian oceanic domains. Geosphere 13 (5), 1664–1712. https://doi.org/10.1130/GES01463.1.
Zuza, A.V., Li, B., Tremblay, M.M., Chen, X.H., Shuster, D.L., Yin, A., 2016. Cenozoic development of the Northern Tibetan Plateau and the onset of thrust and strike-slip faulting: constraints from apatite and zircon (U-Th)/He and fission-track thermochronometry. AGU Fall Meet. Abstr. T11A–2586.
Zuza, A.V., Wu, C., Reith, R.C., Yin, A., Liu, W., 2018. Tectonic evolution of the Qilian Shan: an early Paleozoic orogen reactivated in the Cenozoic. Geol. Soc. Am. Bull. 130 (5/6), 881–925. https://doi.org/10.1130/B31721.1.
Zuza, A.V., Wu, C., Wang, Z.Z., Levy, A.A., Li, B., Xiong, X.S., Chen, X.H., 2019. Underthrusting and duplexing beneath the northern Tibetan Plateau and the evolution of the Himalayan-Tibetan orogen. Lithosphere 11 (2), 209–231. https://doi.org/10.1130/L1042.1.